Quantum Langevin theory for two coupled phase-conjugated electromagnetic waves

Yue Jiang[1,2,*] Yefeng Mei[3,†] and Shengwang Du[4,‡]

[1]*JILA, National Institute of Standards and Technology and the University of Colorado, Boulder, Colorado 80309, USA*
[2]*Department of Physics, University of Colorado, Boulder, Colorado 80309, USA*
[3]*Department of Physics, University of Michigan, Ann Arbor, Michigan 48109, USA*
[4]*Department of Physics, The University of Texas at Dallas, Richardson, Texas 75080, USA*

We provide a general macroscopic phenomenological formula of quantum Langevin equations for two coupled phase-conjugated electromagnetic fields with linear loss (gain) and complex nonlinear coupling coefficient. The macroscopic phenomenological formula is obtained from the coupling matrix to preserve the field commutation relations and correlations, which does not require knowing the microscopic details of light-matter interaction and internal atomic structures. To validate this phenomenological formula, we take spontaneous four-wave mixing in a double-Λ four-level atomic system as an example to numerically confirm that our macroscopic phenomenological result is consistent with that obtained from the microscopic Heisenberg-Langevin theory. We find that a complex-valued nonlinear coupling coefficient can lead to noises even without linear gain or loss. Finally, we apply the quantum Langevin equations to study the effects of linear gain and loss, complex phase mismatching, as well as complex nonlinear coupling coefficient in entangled photon pair (biphoton) generation, particularly to their temporal quantum correlations.

I. INTRODUCTION

Quantum Langevin equations is a common approach to studying an open quantum system involving loss or gain, where the stochastic coupling between the system and its environment is molded as a set of Langevin noise operators [1–5]. For example, in the parametric down-conversion (PDC) process, a pump laser beam passes through a $\chi^{(2)}$ nonlinear crystal and is down-converted into a pair of phase-conjugated electromagnetic (EM) waves. In the simplest case with the perfect phase-matching condition and an undepleted pump beam, without linear loss or gain, the two phase-conjugated single-mode fields are governed by the following coupled equations [6]:

$$\frac{\partial}{\partial z}\begin{bmatrix} \hat{a}_1 \\ \hat{a}_2^\dagger \end{bmatrix} = M \begin{bmatrix} \hat{a}_1 \\ \hat{a}_2^\dagger \end{bmatrix} = \begin{bmatrix} 0 & i\kappa \\ -i\kappa & 0 \end{bmatrix} \begin{bmatrix} \hat{a}_1 \\ \hat{a}_2^\dagger \end{bmatrix}, \qquad (1)$$

where $\hat{a}_m$ and $\hat{a}_m^\dagger$ ($m = 1, 2$) are the field annihilation and creation operators, M is the 2×2 coupling matrix, and κ is the (real) nonlinear coupling coefficient. Here we consider only the forward-wave case with both fields propagating along the same $+z$ direction. If losses are presented during the propagation of the two fields, the coupling matrix is

$$M = \begin{bmatrix} -\alpha_1 & i\kappa \\ -i\kappa & -\alpha_2 \end{bmatrix}, \qquad (2)$$

and their coupled equations become [3,7]

$$\frac{\partial}{\partial z}\begin{bmatrix} \hat{a}_1 \\ \hat{a}_2^\dagger \end{bmatrix} = \begin{bmatrix} -\alpha_1 & i\kappa \\ -i\kappa & -\alpha_2 \end{bmatrix}\begin{bmatrix} \hat{a}_1 \\ \hat{a}_2^\dagger \end{bmatrix} + \begin{bmatrix} \sqrt{2\alpha_1}\hat{f}_1 \\ \sqrt{2\alpha_2}\hat{f}_2^\dagger \end{bmatrix}, \qquad (3)$$

where $\alpha_m > 0$ are the loss (absorption) coefficients, and $\hat{f}_m$ are the associated Langevin noise operators satisfying $[\hat{f}_m(\omega, z), \hat{f}_n^\dagger(\omega', z')] = \delta_{mn}\delta(\omega - \omega')\delta(z - z')$. If there is linear gain instead of loss, for example, in channel 1, i.e., $\alpha_1 < 0$, Eq. (3) can be modified by taking $\sqrt{2\alpha_1}\hat{f}_1 \rightarrow \sqrt{-2\alpha_1}\hat{f}_1^\dagger$. One can show that these Langevin noise operators are necessary to preserve the commutation relations during propagation, i.e. $[\hat{a}_m(\omega, z), \hat{a}_n^\dagger(\omega', z)] = [\hat{a}_m(\omega, 0), \hat{a}_n^\dagger(\omega', 0)] = \delta_{mn}\delta(\omega - \omega')$.

Equation (3) has been widely applied for PDC processes where the nonlinear coupling coefficient κ is real [3,7–9]. However, in a more general case of coupled phase-conjugated fields, such as four-wave mixing (FWM) near atomic resonances [10–12], the nonlinear coupling coefficient κ can take a complex value involving complicated atomic transitions. In this case, Eq. (3) is not valid and its solution does not preserve commutation relations of the fields. What are the general quantum Langevin coupled equations accounting for the complex nonlinear coupling coefficient?

To answer the question, the common approach is to derive quantum Langevin equations by solving the light-matter coupled Heisenberg equations, which requires knowing microscopic details of light-matter interaction such as atomic populations and transitions [11–13]. The complexity of this approach increases dramatically as more atomic transitions are involved and it is extremely difficult for experimentalists to follow, particularly in some situations where it is impossible to obtain full microscopic details. Then our

*yue.jiang@jila.colorado.edu
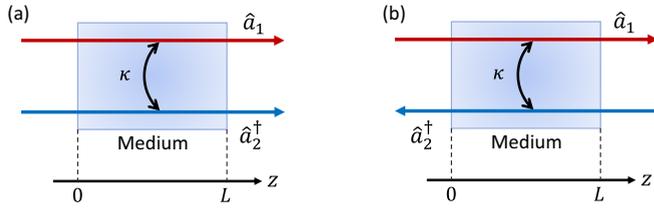†meiyf@umich.edu
‡dusw@utdallas.edu

FIG. 1. Schematics of two coupled phase-conjugated electromagnetic waves: (a) forward-wave configuration, and (b) backward-wave configuration. κ is the nonlinear coupling coefficient between the two modes.

reduced question becomes: Is it possible to obtain self-consistent quantum Langevin coupled equations from the general expression of the coupling matrix? We call this the macroscopic phenomenological approach. We wish to investigate Langevin noises induced by a complex nonlinear coupling coefficient κ.

In this article we provide a general macroscopic phenomenological formula of quantum Langevin equations for two coupled phase-conjugated fields with linear loss (gain) and complex nonlinear coupling coefficient, in both forward- and backward-wave configurations. The macroscopic phenomenological formula is obtained from the coupling matrix by preserving commutation relations and correlations of the fields, which does not require knowing the microscopic details of light-matter interaction and internal atomic structures. We aim to make it readable and accessible for experimental researchers in the quantum optics community.

This article is structured as follows. In Sec. II, to fulfill the requirement of preserving commutation relations, we formulate the general macroscopic phenomenological quantum Langevin coupled equations and their solutions from the coupling matrix, taking into account linear loss (gain) and complex nonlinear coupling coefficient, in both forward- and backward-wave configurations. In Sec. III, taking spontaneous four-wave mixing (SFWM) in a double-Λ four-level atomic system as an example, we derive the coupled Langevin equations from microscopic light-atom Heisenberg interaction for this special case. We numerically confirm that the macroscopic phenomenological solution in Sec. II agrees well with the microscopic approach. In Sec. IV, we apply the quantum Langevin theory to study effects of linear gain and loss, complex phase mismatching, and complex nonlinear coupling coefficient in entangled photon pair (biphoton) generation, particularly to their temporal quantum correlations. We conclude in Sec. V.

II. QUANTUM LANGEVIN EQUATIONS

Here we consider the two coupled single-mode phase-conjugated fields in either forward-wave or backward-wave configuration, as illustrated in Fig. 1. In the forward-wave configuration [Fig. 1(a)], both fields propagate along the $+z$ direction through a nonlinear medium with a length L. In the backward-wave configuration [Fig. 1(b)], the two fields propagate in opposing directions. The field annihilation operators

$\hat{a}_m(t, z)$ can be expressed as

$$\hat{a}_1(t, z) = \frac{1}{\sqrt{2\pi}} \int d\omega \, \hat{a}_1(\omega, z) e^{i(\frac{\omega}{c}z - \omega t)},$$
$$\hat{a}_2(t, z) = \frac{1}{\sqrt{2\pi}} \int d\omega \, \hat{a}_2(\omega, z) e^{i(\pm \frac{\omega}{c}z - \omega t)}, \quad (4)$$

where $\pm$ represents that field 2 propagates along the $+z$ or $-z$ direction, for the forward-wave or backward-wave configuration, respectively. The filed operators satisfy the following commutation relations:

$$[\hat{a}_m(t, z), \hat{a}_n^\dagger(t', z)] = \delta_{mn}\delta(t - t'),$$
$$[\hat{a}_m(\omega, z), \hat{a}_n^\dagger(\omega', z)] = \delta_{mn}\delta(\omega - \omega'). \quad (5)$$

In the forward-wave configuration, both fields are input at $z = 0$, or $\hat{a}_1(0)$ and $\hat{a}_2(0)$ are the "initial" boundary conditions. The general coupling matrix is [14]

$$M_F = \begin{bmatrix} -\alpha_1 + i\frac{\Delta k}{2} & i\kappa \\ -i\kappa & -\alpha_2^* - i\frac{\Delta k}{2} \end{bmatrix}, \quad (6)$$

where $\alpha_m = -i\frac{\omega_m}{2c}\chi_m$ with χ_m being linear susceptibility, and Δk (real) is the phase mismatching in vacuum. In general, α_m is complex valued, whose real part $\text{Re}\{\alpha_m\} > 0$ represents loss (or gain for $\text{Re}\{\alpha_m\} < 0$) and imaginary part represents phase velocity dispersion. The nonlinear coupling coefficient κ can also be complex valued. In the backward-wave configuration, the general coupling matrix becomes [12,15]

$$M_B = \begin{bmatrix} -\alpha_1 + i\frac{\Delta k}{2} & i\kappa \\ i\kappa & \alpha_2^* - i\frac{\Delta k}{2} \end{bmatrix}, \quad (7)$$

and the "initial" boundary conditions are $\hat{a}_1(0)$ and $\hat{a}_2(L)$: field 1 is input at $z = 0$ and field 2 is input at $z = L$.

One can show that, under the unitary gauge transformation

$$\begin{bmatrix} \hat{a}_1 \\ \hat{a}_2^\dagger \end{bmatrix} = \begin{bmatrix} e^{i\theta/2} & 0 \\ 0 & e^{-i\theta/2} \end{bmatrix} \begin{bmatrix} \hat{a}_1 \\ \hat{a}_2^\dagger \end{bmatrix} = U \begin{bmatrix} \hat{a}_1 \\ \hat{a}_2^\dagger \end{bmatrix} = \begin{bmatrix} \hat{a}_1 e^{i\theta/2} \\ \hat{a}_2^\dagger e^{-i\theta/2} \end{bmatrix}, \quad (8)$$

the corresponding coupling matrices become

$$M_F(\theta) = U M_F U^\dagger = \begin{bmatrix} -\alpha_1 + i\frac{\Delta k}{2} & i\kappa e^{i\theta} \\ -i\kappa e^{-i\theta} & -\alpha_2^* - i\frac{\Delta k}{2} \end{bmatrix} \quad (9)$$

and

$$M_B(\theta) = U M_B U^\dagger = \begin{bmatrix} -\alpha_1 + i\frac{\Delta k}{2} & i\kappa e^{i\theta} \\ i\kappa e^{-i\theta} & \alpha_2^* - i\frac{\Delta k}{2} \end{bmatrix}. \quad (10)$$

As physics is preserved and unchanged under the above gauge transformation, we take $\theta = 0$ throughout this article for convenience and simplification.

In the presence of linear loss or gain, i.e., $\text{Re}\{\alpha_m\} \neq 0$, or complex nonlinear coupling coefficient, $\kappa \neq \kappa^*$, the two-mode coupled equations must include Langevin noise operators to preserve the commutation relations of the field operators in Eq. (5). The noise operators should only be related to $\text{Re}\{\alpha_m\}$ and $\text{Im}\{\kappa\}$. As κ is real, the coupled equations in forward-wave configuration should be reduced to the known Eq. (3). For both forward- and backward-wave configurations in the same nonlinear material, the noise origin is the same except field 2 propagates along the $\pm z$ direction

for different configurations. With these guidelines, we provide quantum Langevin equations for the two phase-conjugated fields from their coupling matrix in the following subsections.

A. Forward-wave configuration

In the forward-wave configuration as shown in Fig. 1(a), we find that its quantum Langevin coupled equations can be expressed in the following general form:

$$\frac{\partial}{\partial z}\begin{bmatrix}\hat{a}_1 \\ \hat{a}_2^\dagger\end{bmatrix} = \mathrm{M_F}\begin{bmatrix}\hat{a}_1 \\ \hat{a}_2^\dagger\end{bmatrix} + \mathrm{N_{FR}}\begin{bmatrix}\hat{f}_1 \\ \hat{f}_2^\dagger\end{bmatrix} + \mathrm{N_{FI}}\begin{bmatrix}\hat{f}_1^\dagger \\ \hat{f}_2\end{bmatrix}, \quad (11)$$

with the "initial" condition at $z = 0$:

$$[\hat{a}_m(\omega, 0), \hat{a}_n^\dagger(\omega', 0)] = \delta_{mn}\delta(\omega - \omega'). \quad (12)$$

The Langevin noise operators satisfy

$$[\hat{f}_m(\omega, z), \hat{f}_n^\dagger(\omega', z')] = \delta_{mn}\delta(\omega - \omega')\delta(z - z') \quad (13)$$

and have the following correlations:

$$\langle \hat{f}_m^\dagger(\omega, z)\hat{f}_n(\omega', z')\rangle = 0,$$
$$\langle \hat{f}_m(\omega, z)\hat{f}_n^\dagger(\omega', z')\rangle = \delta_{mn}\delta(\omega - \omega')\delta(z - z'), \quad (14)$$
$$\langle \hat{f}_m(\omega, z)\hat{f}_n(\omega', z')\rangle = \langle \hat{f}_m^\dagger(\omega, z)\hat{f}_n^\dagger(\omega', z')\rangle = 0.$$

The Langevin noise matrix is given by

$$\mathrm{N_F} \equiv \sqrt{-(\mathrm{M_F} + \mathrm{M_F^*})} = \mathrm{N_{FR}} + i\mathrm{N_{FI}}, \quad (15)$$

where $\mathrm{N_{FR}}$ and $\mathrm{N_{FI}}$ are the real and imaginary parts of the matrix $\mathrm{N_F}$ (i.e., $\mathrm{N_{F}}_{mn} = \mathrm{N_{FR}}_{mn} + i\mathrm{N_{FI}}_{mn}$), respectively. As indicated in Eq. (14), in this work we make the physical assumption that the noises fluctuate about a mean value of zero, i.e., the noise sources are in their ground states, such that their mean occupation numbers are zero.

We obtain the solution of Eq. (11) at the output surface $z = L$ as the following:

$$\begin{bmatrix}\hat{a}_1(L) \\ \hat{a}_2^\dagger(L)\end{bmatrix} = e^{\mathrm{M_F}L}\begin{bmatrix}\hat{a}_1(0) \\ \hat{a}_2^\dagger(0)\end{bmatrix} + \int_0^L e^{\mathrm{M_F}(L-z)}\left(\mathrm{N_{FR}}\begin{bmatrix}\hat{f}_1(z) \\ \hat{f}_2^\dagger(z)\end{bmatrix}\right.$$
$$\left. + \mathrm{N_{FI}}\begin{bmatrix}\hat{f}_1^\dagger(z) \\ \hat{f}_2(z)\end{bmatrix}\right)dz. \quad (16)$$

Defining

$$e^{\mathrm{M_F}L} \equiv \begin{bmatrix}A & B \\ C & D\end{bmatrix}, \quad (17)$$

$$e^{\mathrm{M_F}(L-z)} \equiv \begin{bmatrix}A_1(z) & B_1(z) \\ C_1(z) & D_1(z)\end{bmatrix}, \quad (18)$$

we rewrite Eq. (16) as

$$\begin{bmatrix}\hat{a}_1(L) \\ \hat{a}_2^\dagger(L)\end{bmatrix} = \begin{bmatrix}A & B \\ C & D\end{bmatrix}\begin{bmatrix}\hat{a}_1(0) \\ \hat{a}_2^\dagger(0)\end{bmatrix}$$
$$+ \int_0^L \begin{bmatrix}A_1(z) & B_1(z) \\ C_1(z) & D_1(z)\end{bmatrix}\left(\mathrm{N_{FR}}\begin{bmatrix}\hat{f}_1(z) \\ \hat{f}_2^\dagger(z)\end{bmatrix}\right.$$
$$\left. + \mathrm{N_{FI}}\begin{bmatrix}\hat{f}_1^\dagger(z) \\ \hat{f}_2(z)\end{bmatrix}\right)dz. \quad (19)$$

We numerically confirm that the solution preserves the commutation relations

$$[\hat{a}_m(\omega, L), \hat{a}_n^\dagger(\omega', L)] = [\hat{a}_m(\omega, 0), \hat{a}_n^\dagger(\omega', 0)]$$
$$= \delta_{mn}\delta(\omega - \omega'). \quad (20)$$

Now we examine some special cases.

Case 1. We first consider the coupling matrix $\mathrm{M_F}$ in Eq. (6) where the nonlinear coupling coefficient κ is real and both modes have losses ($\mathrm{Re}\{\alpha_m\} \geqslant 0$). This works for most PDC processes [3,7]. Under such a condition, we have the following diagonalized noise matrix:

$$\mathrm{N_F} = \mathrm{N_{FR}} = \begin{bmatrix}\sqrt{2\mathrm{Re}\{\alpha_1\}} & 0 \\ 0 & \sqrt{2\mathrm{Re}\{\alpha_2\}}\end{bmatrix}, \quad (21)$$

and the coupled Langevin equations

$$\frac{\partial}{\partial z}\begin{bmatrix}\hat{a}_1 \\ \hat{a}_2^\dagger\end{bmatrix} = \mathrm{M_F}\begin{bmatrix}\hat{a}_1 \\ \hat{a}_2^\dagger\end{bmatrix} + \begin{bmatrix}\sqrt{2\mathrm{Re}\{\alpha_1\}}\hat{f}_1 \\ \sqrt{2\mathrm{Re}\{\alpha_2\}}\hat{f}_2^\dagger\end{bmatrix}, \quad (22)$$

which is the well-known result in literature [3,7].

Case 2. κ is real, mode 1 has linear loss ($\mathrm{Re}\{\alpha_1\} = \alpha \geqslant 0$), and mode 2 has linear gain ($\mathrm{Re}\{\alpha_2\} = -g \leqslant 0$). The noise matrix becomes

$$\mathrm{N_F} = \begin{bmatrix}\sqrt{2\alpha} & 0 \\ 0 & i\sqrt{2g}\end{bmatrix}. \quad (23)$$

We have the following coupled Langevin equations:

$$\frac{\partial}{\partial z}\begin{bmatrix}\hat{a}_1 \\ \hat{a}_2^\dagger\end{bmatrix} = \mathrm{M_F}\begin{bmatrix}\hat{a}_1 \\ \hat{a}_2^\dagger\end{bmatrix} + \begin{bmatrix}\sqrt{2\alpha}\hat{f}_1 \\ \sqrt{2g}\hat{f}_2\end{bmatrix}. \quad (24)$$

Case 3. The two modes are perfectly phase-matched without linear gain or loss: $\Delta k = 0$, $\alpha_1 = \alpha_2 = 0$, but the nonlinear coupling coefficient is complex-valued $\kappa = \eta + i\zeta$. In this case, the coupled matrix is

$$\mathrm{M_F} = \begin{bmatrix}0 & -\zeta + i\eta \\ \zeta - i\eta & 0\end{bmatrix}. \quad (25)$$

The noise matrix becomes

$$\mathrm{N_F} = \Theta(\zeta)\sqrt{\zeta}\begin{bmatrix}1 & 1 \\ -1 & 1\end{bmatrix} + i\Theta(-\zeta)\sqrt{-\zeta}\begin{bmatrix}1 & 1 \\ -1 & 1\end{bmatrix}, \quad (26)$$

where $\Theta(\zeta)$ is the Heaviside step function, $\Theta(\zeta) = 1$ if $\zeta > 0$, and $\Theta(\zeta) = 0$ if $\zeta \leqslant 0$. The Langevin coupled equations are

$$\frac{\partial}{\partial z}\begin{bmatrix}\hat{a}_1 \\ \hat{a}_2^\dagger\end{bmatrix} = \mathrm{M_F}\begin{bmatrix}\hat{a}_1 \\ \hat{a}_2^\dagger\end{bmatrix} + \Theta(\zeta)\sqrt{\zeta}\begin{bmatrix}1 & 1 \\ -1 & 1\end{bmatrix}\begin{bmatrix}\hat{f}_1 \\ \hat{f}_2^\dagger\end{bmatrix}$$
$$+ \Theta(-\zeta)\sqrt{-\zeta}\begin{bmatrix}1 & 1 \\ -1 & 1\end{bmatrix}\begin{bmatrix}\hat{f}_1^\dagger \\ \hat{f}_2\end{bmatrix}. \quad (27)$$

Equation (27) shows that a complex-valued nonlinear coupling coefficient also leads to Langevin noises even when there is no linear gain or loss. This is revealed by this article for the first time.

Case 4. As κ is real and there is no linear loss or gain ($\alpha_1 = \alpha_2 = 0$), the coupled equations can be written as

$$i\frac{\partial}{\partial z}\begin{bmatrix}\hat{a}_1 \\ \hat{a}_2^\dagger\end{bmatrix} = \begin{bmatrix}-\frac{\Delta k}{2} & -\kappa \\ \kappa & \frac{\Delta k}{2}\end{bmatrix}\begin{bmatrix}\hat{a}_1 \\ \hat{a}_2^\dagger\end{bmatrix} = \hat{\mathcal{H}}\begin{bmatrix}\hat{a}_1 \\ \hat{a}_2^\dagger\end{bmatrix}. \quad (28)$$

The effective Hamiltonian $\hat{\mathcal{H}}$ has anti-parity-time (APT) symmetry, which has been demonstrated in FWM in cold atoms [14,16].

B. Backward-wave configuration

In the back-wave configuration as shown in Fig. 1(b), the quantum Langevin coupled equations can be expressed in the following general form:

$$\frac{\partial}{\partial z}\begin{bmatrix} \hat{a}_1 \\ \hat{a}_2^\dagger \end{bmatrix} = M_B \begin{bmatrix} \hat{a}_1 \\ \hat{a}_2^\dagger \end{bmatrix} + N_{BR}\begin{bmatrix} \hat{f}_1 \\ \hat{f}_2^\dagger \end{bmatrix} + N_{BI}\begin{bmatrix} \hat{f}_1^\dagger \\ \hat{f}_2 \end{bmatrix}. \quad (29)$$

Different from the forward-wave configuration, the "boundary" condition is

$$[\hat{a}_1(\omega, 0), \hat{a}_1^\dagger(\omega', 0)] = [\hat{a}_2(\omega, L), \hat{a}_2^\dagger(\omega', L)] = \delta(\omega - \omega'). \quad (30)$$

The Langevin noise operators satisfy the same commutation relations and correlations in Eqs. (13) and (14). The Langevin noise matrix is given by

$$N_B \equiv \begin{bmatrix} 1 & 0 \\ 0 & -1 \end{bmatrix} \sqrt{\begin{bmatrix} -M_{B11} & -M_{B12} \\ M_{B21} & M_{B22} \end{bmatrix} + \begin{bmatrix} -M_{B11} & -M_{B12} \\ M_{B21} & M_{B22} \end{bmatrix}^*}$$

$$= N_{BR} + iN_{BI}, \quad (31)$$

where N_{BR} and N_{BI} are the real and imaginary parts of the matrix N_B, respectively. One can show that the noise matrix

defined in Eq. (31) has the same origin as that in the forward-wave configuration in the same nonlinear material:

$$N_B = \begin{bmatrix} 1 & 0 \\ 0 & -1 \end{bmatrix} N_F. \quad (32)$$

We note that the choice of noise matrix is not unique. For example, transformation $\hat{f}_1 \rightarrow -\hat{f}_1$ or/and $\hat{f}_2 \rightarrow -\hat{f}_2$ does not affect computing any physical observable. We elaborate on this more in Appendix A.

We obtain the solution of Eq. (29) at $z = L$ as the following:

$$\begin{bmatrix} \hat{a}_1(L) \\ \hat{a}_2^\dagger(L) \end{bmatrix} = e^{M_B L}\begin{bmatrix} \hat{a}_1(0) \\ \hat{a}_2^\dagger(0) \end{bmatrix} + \int_0^L e^{M_B(L-z)}\left(N_{BR}\begin{bmatrix} \hat{f}_1(z) \\ \hat{f}_2^\dagger(z) \end{bmatrix} \right.$$

$$\left. + N_{BI}\begin{bmatrix} \hat{f}_1^\dagger(z) \\ \hat{f}_2(z) \end{bmatrix} \right) dz. \quad (33)$$

We define

$$e^{M_B L} \equiv \begin{bmatrix} \bar{A} & \bar{B} \\ \bar{C} & \bar{D} \end{bmatrix}, \quad (34)$$

$$e^{M_B(L-z)} \equiv \begin{bmatrix} \bar{A}_1(z) & \bar{B}_1(z) \\ \bar{C}_1(z) & \bar{D}_1(z) \end{bmatrix}. \quad (35)$$

Different from the forward-wave case, in the backward-wave configuration, the mode 1 input is at $z = 0$ and the mode 2 input is at $z = L$. With known $\hat{a}_1(0)$ and $\hat{a}_2(L)$, we rearrange Eq. (33) and obtain solutions for $\hat{a}_1(L)$ and $\hat{a}_2(0)$:

$$\begin{bmatrix} \hat{a}_1(L) \\ \hat{a}_2^\dagger(0) \end{bmatrix} = \begin{bmatrix} A & B \\ C & D \end{bmatrix}\begin{bmatrix} \hat{a}_1(0) \\ \hat{a}_2^\dagger(L) \end{bmatrix} + \begin{bmatrix} 1 & -B \\ 0 & -D \end{bmatrix}\int_0^L \begin{bmatrix} \bar{A}_1(z) & \bar{B}_1(z) \\ \bar{C}_1(z) & \bar{D}_1(z) \end{bmatrix}\left(N_{BR}\begin{bmatrix} \hat{f}_1(z) \\ \hat{f}_2^\dagger(z) \end{bmatrix} + N_{BI}\begin{bmatrix} \hat{f}_1^\dagger(z) \\ \hat{f}_2(z) \end{bmatrix} \right) dz, \quad (36)$$

where

$$A = \bar{A} - \frac{\bar{B}\bar{C}}{\bar{D}},$$

$$B = \frac{\bar{B}}{\bar{D}},$$

$$C = -\frac{\bar{C}}{\bar{D}}, \quad (37)$$

$$D = \frac{1}{\bar{D}}.$$

We numerically confirm that Eq. (36) preserves the commutation relations

$$[\hat{a}_1(\omega, L), \hat{a}_1^\dagger(\omega', L)] = [\hat{a}_1(\omega, 0), \hat{a}_1^\dagger(\omega', 0)],$$

$$[\hat{a}_2(\omega, 0), \hat{a}_2^\dagger(\omega', 0)] = [\hat{a}_2(\omega, L), \hat{a}_2^\dagger(\omega', L)]. \quad (38)$$

Similarly to the forward-wave configuration, we examine the following four special cases.

Case 1. We assume the nonlinear coupling coefficient κ is real and both modes have losses ($\text{Re}\{\alpha_m\} \geqslant 0$). Under such a condition, we have the following diagonalized noise matrix:

$$N_B = \begin{bmatrix} \sqrt{2\text{Re}\{\alpha_1\}} & 0 \\ 0 & -\sqrt{2\text{Re}\{\alpha_2\}} \end{bmatrix}, \quad (39)$$

and the coupled Langevin equations

$$\frac{\partial}{\partial z}\begin{bmatrix} \hat{a}_1 \\ \hat{a}_2^\dagger \end{bmatrix} = M_B \begin{bmatrix} \hat{a}_1 \\ \hat{a}_2^\dagger \end{bmatrix} + \begin{bmatrix} \sqrt{2\text{Re}\{\alpha_1\}}\hat{f}_1 \\ -\sqrt{2\text{Re}\{\alpha_2\}}\hat{f}_2^\dagger \end{bmatrix}. \quad (40)$$

Case 2. κ is real, mode 1 has linear loss ($\text{Re}\{\alpha_1\} = \alpha \geqslant 0$), and mode 2 has linear gain ($\text{Re}\{\alpha_2\} = -g \leqslant 0$). The noise matrix becomes

$$N_F = \begin{bmatrix} \sqrt{2\alpha} & 0 \\ 0 & -i\sqrt{2g} \end{bmatrix}. \quad (41)$$

We have the following coupled Langevin equations:

$$\frac{\partial}{\partial z}\begin{bmatrix} \hat{a}_1 \\ \hat{a}_2^\dagger \end{bmatrix} = M_B \begin{bmatrix} \hat{a}_1 \\ \hat{a}_2^\dagger \end{bmatrix} + \begin{bmatrix} \sqrt{2\alpha}\hat{f}_1 \\ -\sqrt{2g}\hat{f}_2 \end{bmatrix}. \quad (42)$$

Case 3. The two modes are perfectly phase matched without linear gain and loss: $\Delta k = 0$, $\alpha_1 = \alpha_2 = 0$, but the nonlinear coupling coefficient is complex-valued $\kappa = \eta + i\zeta$. In this case, the coupled matrix is

$$M_B = \begin{bmatrix} 0 & -\zeta + i\eta \\ -\zeta + i\eta & 0 \end{bmatrix}. \quad (43)$$

The noise matrix becomes

$$
N_B = \Theta(\zeta)\sqrt{\zeta}\begin{bmatrix} 1 & 1 \\ 1 & -1 \end{bmatrix} + i\Theta(-\zeta)\sqrt{-\zeta}\begin{bmatrix} 1 & 1 \\ 1 & -1 \end{bmatrix}. \quad (44)
$$

The Langevin coupled equations are

$$
\frac{\partial}{\partial z}\begin{bmatrix} \hat{a}_1 \\ \hat{a}_2^\dagger \end{bmatrix} = M_B \begin{bmatrix} \hat{a}_1 \\ \hat{a}_2^\dagger \end{bmatrix} + \Theta(\zeta)\sqrt{\zeta}\begin{bmatrix} 1 & 1 \\ 1 & -1 \end{bmatrix}\begin{bmatrix} \hat{f}_1 \\ \hat{f}_2^\dagger \end{bmatrix}
$$
$$
+ \Theta(-\zeta)\sqrt{-\zeta}\begin{bmatrix} 1 & 1 \\ 1 & -1 \end{bmatrix}\begin{bmatrix} \hat{f}_1^\dagger \\ \hat{f}_2 \end{bmatrix}. \quad (45)
$$

Equation (45) shows that in the backward-wave configuration, a complex-valued nonlinear coupling coefficient also leads to Langevin noises even though there is no linear gain or loss.

Case 4. As κ is real and there are equal losses in both modes ($\alpha_1 = \alpha_2 = \alpha > 0$) with perfect phase matching ($\Delta k = 0$), the coupled equations can be written as

$$
i\frac{\partial}{\partial z}\begin{bmatrix} \hat{a}_1 \\ \hat{a}_2^\dagger \end{bmatrix} = \begin{bmatrix} -i\alpha & -\kappa \\ -\kappa & i\alpha \end{bmatrix}\begin{bmatrix} \hat{a}_1 \\ \hat{a}_2^\dagger \end{bmatrix} = \hat{\mathcal{H}}\begin{bmatrix} \hat{a}_1 \\ \hat{a}_2^\dagger \end{bmatrix}. \quad (46)
$$

Interestingly, the effective Hamiltonian $\hat{\mathcal{H}}$ here follows parity-time (PT) symmetry [17,18].

III. MICROSCOPIC ORIGIN OF LANGEVIN NOISES: SFWM

One could validate the above phenomenological approach of quantum Langevin coupled equations by confirming the microscopic origin of the Langevin noises. However, for two systems with the same quantum Langevin equations, their microscopic structures may be quite different. Therefore, it is impossible to sort all microscopic systems. In this section, we focus on SFWM in a double-Λ four-level atomic system [10–12,19,20] with electromagnetically induced transparency (EIT) [21,22], and show that the phenomenological approach in the above section agrees with the numerical results from the microscopic quantum theory of light-atom interaction.

We start from a single-atom picture, considering an EM wave couples the atomic transition $|j\rangle$ and $|k\rangle$. The induced single-atom polarization $\hat{p}_{jk} \propto \mu_{jk}\hat{\sigma}_{jk}$, where μ_{jk} is the electric dipole moment matrix element, $\hat{\sigma}_{jk} = |j\rangle\langle k|$ is a single-atom transition operator from state $|k\rangle$ to $|j\rangle$. In the Heisenberg-Langevin picture, the single-atom transition operator can be expressed as

$$
\hat{\sigma}_{jk} = \hat{\sigma}_{jk}^{(0)} + \sum_{\mu\nu}\beta_{\mu\nu}\hat{f}_{\mu\nu}^{(\sigma)}, \quad (47)
$$

where $\hat{\sigma}_{jk}^{(0)} = \langle\hat{\sigma}_{jk}\rangle$ is the zeroth-order steady-state solution. The single atom noise operator between atomic transition $|\nu\rangle \to |\mu\rangle$ is represented by $\hat{f}_{\mu\nu}^{(\sigma)}$, which satisfies the following correlations:

$$
\langle\hat{f}_{\mu\nu}^{(\sigma)}(\omega)\hat{f}_{\mu'\nu'}^{(\sigma)\dagger}(\omega')\rangle = \langle\hat{f}_{\mu\nu}^{(\sigma)}(\omega)\hat{f}_{\nu'\mu'}^{(\sigma)}(\omega')\rangle
$$
$$
= \mathcal{D}_{\mu\nu,\nu'\mu'}\delta(\omega-\omega'),
$$
$$
\langle\hat{f}_{\mu\nu}^{(\sigma)\dagger}(\omega)\hat{f}_{\mu'\nu'}^{(\sigma)}(\omega')\rangle = \langle\hat{f}_{\nu\mu}^{(\sigma)}(\omega)\hat{f}_{\mu'\nu'}^{(\sigma)}(\omega')\rangle
$$
$$
= \mathcal{D}_{\nu\mu,\mu'\nu'}\delta(\omega-\omega'), \quad (48)
$$

where $\mathcal{D}_{\mu\nu,\nu'\mu'}$ and $\mathcal{D}_{\nu\mu,\mu'\nu'}$ are diffusion coefficients.

In a continuous medium with atomic number density n, the noises from different atoms are uncorrelated. We have the spatially averaged atomic operator

$$
\hat{\bar{\sigma}}_{jk} \equiv \hat{\sigma}_{jk}^{(0)} + \frac{1}{\sqrt{nA}}\sum_{\mu\nu}\beta_{\mu\nu}\hat{\bar{f}}_{\mu\nu}^{(\sigma)}, \quad (49)
$$

where A is the single-mode cross-section area, and the spatially averaged atomic noise operators $\hat{\bar{f}}_{\mu\nu}^{(\sigma)}$ satisfy the following modified correlations:

$$
\langle\hat{\bar{f}}_{\mu\nu}^{(\sigma)}(\omega,z)\hat{\bar{f}}_{\mu'\nu'}^{(\sigma)\dagger}(\omega',z')\rangle = \langle\hat{\bar{f}}_{\mu\nu}^{(\sigma)}(\omega,z)\hat{\bar{f}}_{\nu'\mu'}^{(\sigma)}(\omega',z')\rangle
$$
$$
= \mathcal{D}_{\mu\nu,\nu'\mu'}\delta(\omega-\omega')\delta(z-z'),
$$
$$
\langle\hat{\bar{f}}_{\mu\nu}^{(\sigma)\dagger}(\omega,z)\hat{\bar{f}}_{\mu'\nu'}^{(\sigma)}(\omega',z')\rangle = \langle\hat{\bar{f}}_{\nu\mu}^{(\sigma)}(\omega,z)\hat{\bar{f}}_{\mu'\nu'}^{(\sigma)}(\omega',z')\rangle
$$
$$
= \mathcal{D}_{\nu\mu,\mu'\nu'}\delta(\omega-\omega')\delta(z-z'), \quad (50)
$$

where the diffusion coefficients are the same as those from the single-atom picture.

The electric field and polarization are described as

$$
\hat{\mathbf{E}}(t,z) = \tfrac{1}{2}[\hat{E}^{(+)}(t,z) + \hat{E}^{(-)}(t,z)],
$$
$$
\hat{\mathbf{P}}(t,z) = \tfrac{1}{2}[\hat{P}^{(+)}(t,z) + \hat{P}^{(-)}(t,z)], \quad (51)
$$

where $\hat{E}^{(+)}, \hat{P}^{(+)}$ and $\hat{E}^{(-)}, \hat{P}^{(-)}$ are positive and negative frequency parts. We take the following Fourier transform:

$$
\hat{E}^{(+)}(t,z) = \frac{1}{\sqrt{2\pi}}\int d\omega \hat{E}(\omega,z)e^{i(\pm\frac{\omega}{c}z-\omega t)},
$$
$$
\hat{P}^{(+)}(t,z) = \frac{1}{\sqrt{2\pi}}\int d\omega \hat{P}(\omega,z)e^{i(\pm\frac{\omega}{c}z-\omega t)}, \quad (52)
$$

where $\hat{E}(\omega,z), \hat{P}(\omega,z)$ are complex amplitudes in the frequency domain. The Maxwell equation under slowly varying envelope approximation (SVEA) can be written as

$$
\pm\frac{\partial\hat{E}(\omega,z)}{\partial z} = \frac{i}{2}\omega\eta\hat{P}(\omega,z), \quad (53)
$$

where $\pm$ represents for propagation direction along $\pm z$, and free space impedance $\eta = 1/(c\varepsilon_0) = 377$ Ohm, with c being the speed of light in vacuum, and ε_0 the vacuum permittivity. With quantized electric field

$$
\hat{E}(\omega,z) = \sqrt{\frac{2\hbar\omega}{c\varepsilon_0 A}}\hat{a}(\omega,z) \quad (54)
$$

and

$$
\hat{P}(\omega,z) = 2n\mu_{jk}\hat{\bar{\sigma}}_{jk}(\omega,z), \quad (55)
$$

we obtain the Langevin equation for the EM field in the atomic medium

$$
\pm\frac{\partial\hat{a}(\omega,z)}{\partial z} = inAg_{jk}\hat{\bar{\sigma}}_{jk}(\omega,z)
$$
$$
= inAg_{jk}\hat{\sigma}_{jk}^{(0)}(\omega,z) + \hat{\bar{F}}(\omega,z), \quad (56)
$$

where

$$
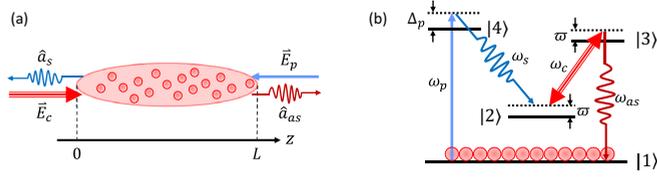g_{jk} = \mu_{jk}\sqrt{\frac{\omega_{jk}}{2c\varepsilon_0\hbar A}},
$$

FIG. 2. Spontaneous four-wave mixing (SFWM) in a double-Λ four-level cold atomic medium. (a) Backward-wave geometry of SFWM optical configuration. Driven by counterpropagating pump (E_p) and coupling (E_c) beams, phase-matched backward Stokes ($\hat{a}_s$) and anti-Stokes ($\hat{a}_{as}$) are spontaneously generated from a laser-cooled atomic medium. (b) Atomic energy-level diagram. The pump (ω_p) laser is detuned with Δ_p from transition $|1\rangle \rightarrow |4\rangle$, and the coupling ($\omega_c$) laser is on-resonant with transition $|2\rangle \rightarrow |3\rangle$. Stokes ($\omega_s$) photons are spontaneously generated from transition $|4\rangle \rightarrow |2\rangle$, and anti-Stokes ($\omega_{as}$) photons from transition $|3\rangle \rightarrow |1\rangle$. $\varpi = \omega_{as} - \omega_{13}$ is the anti-Stokes photon frequency detuning from transition $|1\rangle \rightarrow |3\rangle$.

$$\hat{\bar{F}}(\omega, z) = i\sqrt{nA}g_{jk}\sum_{\mu\nu}\beta_{\mu\nu}\hat{\bar{f}}_{\mu\nu}^{(\sigma)}(\omega, z)$$

$$= i\mu_{jk}\sqrt{\frac{n\omega_{jk}}{2c\varepsilon_0\hbar}}\sum_{\mu\nu}\beta_{\mu\nu}\hat{\bar{f}}_{\mu\nu}^{(\sigma)}(\omega, z). \tag{57}$$

Here $g_{jk} = g_{kj}^*$ is single-photon-atom coupling strength.

Now we turn to the backward-wave SFWM in a double-Λ four-level atomic system as illustrated in Fig. 2. In the presence of a counterpropagating pump (E_p, ω_p) and coupling (E_c, ω_c) laser beams, phase-matched Stokes (ω_s) and anti-Stokes (ω_{as}) are spontaneously generated and propagate through the medium in opposing directions. In the rotat-

ing reference frame, the interaction Hamiltonian for a single atom is

$$\hat{V} = -\hbar(g_{31}\hat{a}_{as}\hat{\sigma}_{31} + g_{13}\hat{a}_{as}^\dagger\hat{\sigma}_{13}) - \hbar(g_{42}\hat{a}_s\hat{\sigma}_{42} + g_{24}\hat{a}_s^\dagger\hat{\sigma}_{24})$$
$$- \frac{1}{2}\hbar(\Omega_c\hat{\sigma}_{32} + \Omega_c^*\hat{\sigma}_{23}) - \frac{1}{2}\hbar(\Omega_p\hat{\sigma}_{41} + \Omega_p^*\hat{\sigma}_{14})$$
$$- \hbar\Delta_p\hat{\sigma}_{44} - \hbar\varpi\hat{\sigma}_{33} - \hbar\varpi\hat{\sigma}_{22}, \tag{58}$$

where $\Omega_c = \mu_{32}E_c/\hbar$ is coupling Rabi frequency. The coupling laser is on-resonant with transition $|2\rangle \rightarrow |3\rangle$. $\Omega_p = \mu_{41}E_p/\hbar$ is the pump Rabi frequency. The pump laser is far detuned from the transition $|1\rangle \rightarrow |4\rangle$ with $\Delta_p = \omega_p - \omega_{14}$ so that the atomic population mainly occupies the ground state $|1\rangle$. We take this ground-state approximation through this section. With continuous-wave pump and coupling driving fields, the energy conservation leads to $\omega_{as} + \omega_s = \omega_c + \omega_p$. Here $\varpi = \omega_{as} - \omega_{13}$ is the anti-Stokes frequency detuning and thus the Stokes frequency detuning is $\omega_s - \omega_{s0} = -\varpi$.

The atomic evolution is governed by the following Heisenberg-Langevin equation [11]:

$$\frac{\partial}{\partial t}\hat{\sigma}_{jk} = \frac{i}{\hbar}[\hat{V}, \hat{\sigma}_{jk}] - \gamma_{jk}\hat{\sigma}_{jk} + r_{jk}^A + \hat{f}_{jk}^{(\sigma)}, \tag{59}$$

where $\gamma_{jk} = \gamma_{kj}$ (nonzero only as $j \neq k$) are dephasing rates, and r_{jk}^A (nonzero only as $j = k$) are the population transfer resulting from spontaneous emission decay. The full equation of motion can be found in Appendix B. The diffusion coefficients $\mathcal{D}_{jk,j'k'}$ can be obtained through the Einstein relation

$$\mathcal{D}_{jk,j'k'} = \frac{\partial}{\partial t}\langle\hat{\sigma}_{jk}\hat{\sigma}_{j'k'}\rangle$$
$$- \langle\hat{A}_{jk}\hat{\sigma}_{j'k'}\rangle - \langle\hat{\sigma}_{jk}\hat{A}_{j'k'}\rangle, \tag{60}$$

where $\hat{A}_{jk} = \frac{\partial}{\partial t}\hat{\sigma}_{jk} - \hat{f}_{jk}^{(\sigma)}$. For the SFWM governed by Eq. (59), we have [11,12]

$$\begin{bmatrix} \mathcal{D}_{12,21} & \mathcal{D}_{12,24} & \mathcal{D}_{12,31} & \mathcal{D}_{12,34} \\ \mathcal{D}_{42,21} & \mathcal{D}_{42,24} & \mathcal{D}_{42,31} & \mathcal{D}_{42,34} \\ \mathcal{D}_{13,21} & \mathcal{D}_{13,24} & \mathcal{D}_{13,31} & \mathcal{D}_{13,34} \\ \mathcal{D}_{43,21} & \mathcal{D}_{43,24} & \mathcal{D}_{43,31} & \mathcal{D}_{43,34} \end{bmatrix}$$

$$= \begin{bmatrix} 2\gamma_{12}\langle\hat{\sigma}_{11}\rangle + \Gamma_{31}\langle\hat{\sigma}_{33}\rangle + \Gamma_{41}\langle\hat{\sigma}_{44}\rangle & \gamma_{12}\langle\hat{\sigma}_{14}\rangle & 0 & 0 \\ \gamma_{12}\langle\hat{\sigma}_{41}\rangle & 0 & 0 & 0 \\ 0 & 0 & \Gamma_3\langle\hat{\sigma}_{11}\rangle + \Gamma_{31}\langle\hat{\sigma}_{33}\rangle + \Gamma_{41}\langle\hat{\sigma}_{44}\rangle & \Gamma_3\langle\hat{\sigma}_{14}\rangle \\ 0 & 0 & \Gamma_3\langle\hat{\sigma}_{41}\rangle & \Gamma_3\langle\hat{\sigma}_{44}\rangle \end{bmatrix}, \tag{61}$$

$$\begin{bmatrix} \mathcal{D}_{21,12} & \mathcal{D}_{21,42} & \mathcal{D}_{21,13} & \mathcal{D}_{21,43} \\ \mathcal{D}_{24,12} & \mathcal{D}_{24,42} & \mathcal{D}_{24,13} & \mathcal{D}_{24,43} \\ \mathcal{D}_{31,12} & \mathcal{D}_{31,42} & \mathcal{D}_{31,13} & \mathcal{D}_{31,43} \\ \mathcal{D}_{34,12} & \mathcal{D}_{34,42} & \mathcal{D}_{34,13} & \mathcal{D}_{34,43} \end{bmatrix}$$

$$= \begin{bmatrix} 2\gamma_{12}\langle\hat{\sigma}_{22}\rangle + \Gamma_{32}\langle\hat{\sigma}_{33}\rangle + \Gamma_{42}\langle\hat{\sigma}_{44}\rangle & 0 & \gamma_{12}\langle\hat{\sigma}_{23}\rangle & 0 \\ 0 & \Gamma_4\langle\hat{\sigma}_{22}\rangle + \Gamma_{32}\langle\hat{\sigma}_{33}\rangle + \Gamma_{42}\langle\hat{\sigma}_{44}\rangle & 0 & \Gamma_4\langle\hat{\sigma}_{23}\rangle \\ \gamma_{12}\langle\hat{\sigma}_{32}\rangle & 0 & 0 & 0 \\ 0 & \Gamma_4\langle\hat{\sigma}_{32}\rangle & 0 & \Gamma_4\langle\hat{\sigma}_{33}\rangle \end{bmatrix}. \tag{62}$$

Solving Eq. (59) under the ground-state approximation $\langle\hat{\sigma}_{11}\rangle \cong 1$ with weak pump excitation $\Delta_p \gg \{\Omega_p, \Gamma_4\}$, we get the single-atom steady-state solutions (with $\mu\nu = 12, 13, 42, 43$)

$$\hat{\sigma}_{13} = \hat{\sigma}_{13}^{(0)} + \sum_{\mu\nu} \beta_{\mu\nu}^{as} \hat{f}_{\mu\nu}^{(\sigma)},$$

$$\hat{\sigma}_{42} = \hat{\sigma}_{42}^{(0)} + \sum_{\mu\nu} \beta_{\mu\nu}^{s} \hat{f}_{\mu\nu}^{(\sigma)}, \tag{63}$$

where

$$\hat{\sigma}_{13}^{(0)} = \frac{4(\varpi + i\gamma_{12})}{T(\varpi)} g_{31} \hat{a}_{as}$$
$$+ \frac{\Omega_c \Omega_p}{T(\varpi)(\Delta_p + i\gamma_{14})} g_{24} \hat{a}_s^\dagger,$$

$$\hat{\sigma}_{42}^{(0)} = \frac{(\varpi + i\gamma_{13})}{T(\varpi)} \frac{|\Omega_p|^2}{(\Delta_p - i\gamma_{24})} \frac{1}{(\Delta_p + i\gamma_{14})} g_{24} \hat{a}_s^\dagger$$
$$+ \frac{\Omega_p^* \Omega_c^*}{T(\varpi)(\Delta_p - i\gamma_{24})} g_{31} \hat{a}_{as}, \tag{64}$$

$$\beta_{12}^{as} = \frac{i2\Omega_c}{T(\varpi)},$$

$$\beta_{13}^{as} = -\frac{i4(\varpi + i\gamma_{12})}{T(\varpi)},$$

$$\beta_{42}^{as} = -\frac{i\Omega_c \Omega_p}{T(\varpi)(\Delta_p - i\gamma_{24})},$$

$$\beta_{43}^{as} = \frac{i2\Omega_p(\varpi + i\gamma_{12})}{T(\varpi)(\Delta_p - i\gamma_{34})},$$

$$\beta_{12}^{s} = \frac{i2(\varpi + i\gamma_{13})}{T(\varpi)} \frac{\Omega_p^*}{(\Delta_p - i\gamma_{24})},$$

$$\beta_{13}^{s} = -\frac{i\Omega_p^* \Omega_c^*}{T(\varpi)(\Delta_p - i\gamma_{24})},$$

$$\beta_{42}^{s} = -\frac{i}{(\Delta_p - i\gamma_{24})},$$

$$\beta_{43}^{s} = -\frac{i\Omega_c^*}{2(\Delta_p - i\gamma_{24})(\Delta_p - i\gamma_{34})}, \tag{65}$$

where $T(\varpi) \equiv |\Omega_c|^2 - 4(\varpi + i\gamma_{13})(\varpi + i\gamma_{12})$. We then obtain the ensemble spatially averaged atomic operators for generating anti-Stokes and Stokes fields from Eq. (49),

$$\hat{\bar{\sigma}}_{13} = \hat{\sigma}_{13}^{(0)} + \frac{1}{\sqrt{nA}} \sum_{\mu\nu} \beta_{\mu\nu}^{as} \hat{\bar{f}}_{\mu\nu}^{(\sigma)},$$

$$\hat{\bar{\sigma}}_{42} = \hat{\sigma}_{42}^{(0)} + \frac{1}{\sqrt{nA}} \sum_{\mu\nu} \beta_{\mu\nu}^{s} \hat{\bar{f}}_{\mu\nu}^{(\sigma)}. \tag{66}$$

For simplicity, we define $\hat{a}_{as}(\varpi, z) \equiv \hat{a}_{as}(\omega_{as0} + \varpi, z)$ and $\hat{a}_s(\varpi, z) \equiv \hat{a}_s(\omega_{s0} - \varpi, z)$. Following the procedures in Eqs. (56) and (57),

$$\frac{\partial \hat{a}_{as}(\varpi, z)}{\partial z} = inAg_{13} \hat{\bar{\sigma}}_{13}(\varpi, z),$$

$$\frac{\partial \hat{a}_s^\dagger(\varpi, z)}{\partial z} = inAg_{42} \hat{\bar{\sigma}}_{42}(\varpi, z), \tag{67}$$

we get coupled equations for the counterpropagating anti-Stokes (propagating along $+z$) and Stokes (propagating along $-z$) fields in the backward-wave configuration,

$$\frac{\partial}{\partial z} \begin{bmatrix} \hat{a}_{as} \\ \hat{a}_s^\dagger \end{bmatrix} = \begin{bmatrix} -\alpha_{as} + i\frac{\Delta k}{2} & i\kappa_{as} \\ i\kappa_s & \alpha_s^* - i\frac{\Delta k}{2} \end{bmatrix} \begin{bmatrix} \hat{a}_{as} \\ \hat{a}_s^\dagger \end{bmatrix} + \begin{bmatrix} \hat{\bar{F}}_{as} \\ -\hat{\bar{F}}_s^\dagger \end{bmatrix}, \tag{68}$$

where

$$\hat{\bar{F}}_{as} = ig_{13}\sqrt{nA}\left[\beta_{12}^{as}\hat{\bar{f}}_{12}^{(\sigma)} + \beta_{13}^{as}\hat{\bar{f}}_{13}^{(\sigma)} + \beta_{42}^{as}\hat{\bar{f}}_{42}^{(\sigma)} + \beta_{43}^{as}\hat{\bar{f}}_{43}^{(\sigma)}\right],$$

$$\hat{\bar{F}}_s^\dagger = -ig_{42}\sqrt{nA}\left[\beta_{12}^{s}\hat{\bar{f}}_{12}^{(\sigma)} + \beta_{13}^{s}\hat{\bar{f}}_{13}^{(\sigma)} + \beta_{42}^{s}\hat{\bar{f}}_{42}^{(\sigma)} + \beta_{43}^{s}\hat{\bar{f}}_{43}^{(\sigma)}\right], \tag{69}$$

and

$$\alpha_{as} = -i\frac{\omega_{as}}{2c} \chi_{as},$$

$$\alpha_s = -i\frac{\omega_s}{2c} \chi_s,$$

$$\kappa_{as} = \frac{\sqrt{\omega_{as}\omega_s}}{2c} \chi_{as}^{(3)} E_p E_c,$$

$$\kappa_s = \frac{\sqrt{\omega_s\omega_{as}}}{2c} \chi_s^{(3)*} E_p^* E_c^*,$$

$$\chi_{as} = \frac{4n|\mu_{13}|^2}{\varepsilon_0 \hbar} \frac{(\varpi + i\gamma_{12})}{T(\varpi)},$$

$$\chi_s = \frac{n|\mu_{24}|^2}{\varepsilon_0 \hbar} \frac{(\varpi - i\gamma_{13})}{T^*(\varpi)} \frac{|\Omega_p|^2}{\Delta_p^2 + \gamma_{14}^2},$$

$$\chi_{as}^{(3)} = \frac{n\mu_{13}\mu_{32}\mu_{24}\mu_{41}}{\varepsilon_0 \hbar^3} \frac{1}{T(\varpi)} \frac{1}{(\Delta_p + i\gamma_{14})},$$

$$\chi_s^{(3)} = \frac{n\mu_{13}\mu_{32}\mu_{24}\mu_{41}}{\varepsilon_0 \hbar^3} \frac{1}{T^*(\varpi)} \frac{1}{(\Delta_p + i\gamma_{14})}. \tag{70}$$

The expressions for $\beta_{\mu\nu}^{as}$ and $\beta_{\mu\nu}^{s}$ are listed in Eqs. (65). $\Delta k = (\omega_{as} - \omega_s)/c - (\vec{k}_c + \vec{k}_p) \cdot \hat{z}$ is the phase mismatching in vacuum. Here the complex α_{as} represents the EIT loss and phase dispersion. α_s^* is the Raman gain and dispersion along the $-z$ propagation direction. One can show that the nonlinear coupling coefficients can be expressed as $\kappa_{as} = \kappa e^{i\theta}$ and $\kappa_s = \kappa e^{-i\theta}$, where

$$\kappa = \frac{\sqrt{\omega_{as}\omega_s}}{2c} \frac{n\mu_{13}\mu_{24}}{\varepsilon_0 \hbar} \left|\frac{\Omega_p\Omega_c}{\Delta_p + i\gamma_{14}}\right| \frac{1}{T(\varpi)}, \tag{71}$$

and θ is the phase of $\Omega_p\Omega_c/(\Delta_p + i\gamma_{14})$. As a result, κ_{as} and κ_s fulfill the gauge transformation discussed in Sec. II. Therefore, to be consistent with the treatment in Sec. II, we rewrite Eq. (68) to

$$\frac{\partial}{\partial z} \begin{bmatrix} \hat{a}_{as} \\ \hat{a}_s^\dagger \end{bmatrix} = M_B \begin{bmatrix} \hat{a}_{as} \\ \hat{a}_s^\dagger \end{bmatrix} + \begin{bmatrix} \hat{F}_{as} \\ -\hat{F}_s^\dagger \end{bmatrix}, \tag{72}$$
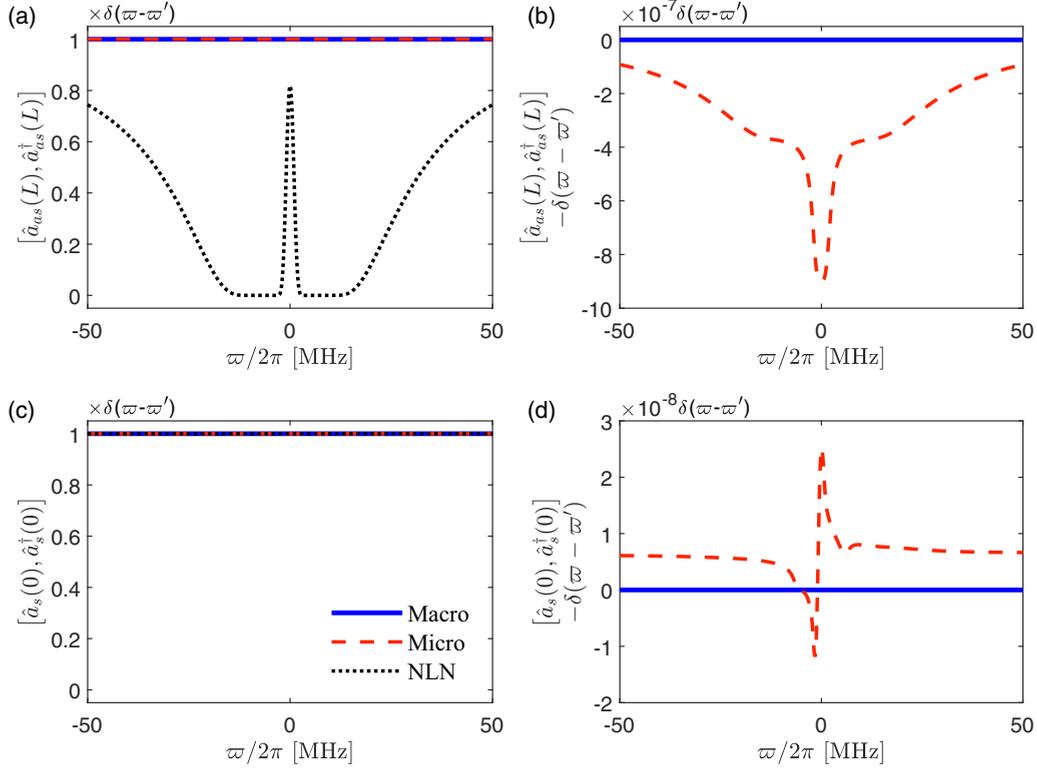
FIG. 3. Comparison of commutation relations between the macroscopic (Macro, blue solid lines) and microscopic (Micro, red dashed lines) approaches in the group delay regime: (a) $[\hat{a}_{as}(L), \hat{a}_{as}^{\dagger}(L)]$, (b) $[\hat{a}_{as}(L), \hat{a}_{as}^{\dagger}(L)] - \delta(\varpi - \varpi')$, (c) $[\hat{a}_{s}(0), \hat{a}_{s}^{\dagger}(0)]$, and (d) $[\hat{a}_{s}(0), \hat{a}_{s}^{\dagger}(0)] - \delta(\varpi - \varpi')$. The results with no Langevin noise operators (NLN) are shown as black dotted lines in (a) and (c).

where

$$
M_B = \begin{bmatrix} -\alpha_{as} + i\frac{\Delta k}{2} & i\kappa \\ i\kappa & \alpha_s^* - i\frac{\Delta k}{2} \end{bmatrix},
$$

$$
\hat{F}_{as} = \hat{\bar{F}}_{as} e^{-i\theta/2},
$$

$$
\hat{F}_s^{\dagger} = \hat{\bar{F}}_s^{\dagger} e^{i\theta/2}. \tag{73}
$$

Similarly, we rewrite the SFWM quantum Langevin equations in the forward-wave configuration in Appendix C.

We now turn to compare Eq. (72) with Eq. (29) from the phenomenological approach in Sec. II, where we take mode 1 as anti-Stokes and mode 2 as Stokes in the backward-wave configuration. From Eq. (29), we have

$$
\hat{F}_{as} = N_{BR11}\hat{f}_1 + N_{BI11}\hat{f}_1^{\dagger} + N_{BI12}\hat{f}_2 + N_{BR12}\hat{f}_2^{\dagger},
$$

$$
\hat{F}_s^{\dagger} = -N_{BR21}\hat{f}_1 - N_{BI21}\hat{f}_1^{\dagger} - N_{BI22}\hat{f}_2 - N_{BR22}\hat{f}_2^{\dagger}. \tag{74}
$$

Therefore, we obtain $\hat{F}_{as}$ and $\hat{F}_s^{\dagger}$ from two different approaches: Eq. (69) from the microscopic photon-atom interaction, and Eq. (74) from the macroscopic phenomenological approach. Although we remark that the atomic noise operators $\hat{\bar{f}}_{\mu\nu}^{(\sigma)}$ are different from the field noise operators $\hat{f}_m$, the correlations of $\hat{F}_{as}$ and $\hat{F}_s$ uniquely determine the system performance. While we find it difficult to analytically prove the two approaches are equivalent, we could numerically compute and compare the commutation relations and correlations of $\hat{a}_{as}, \hat{a}_{as}^{\dagger}, \hat{a}_s$, and $\hat{a}_s^{\dagger}$.

We consider here the backward-wave SFWM in laser-cooled ^{85}Rb atoms with relevant atomic energy levels being $|1\rangle = |5\,^2S_{1/2}, F = 2\rangle$, $|2\rangle = |5\,^2S_{1/2}, F = 3\rangle$, $|3\rangle = |5\,^2P_{1/2}, F = 3\rangle$, and $|4\rangle = |5\,^2P_{3/2}, F = 3\rangle$. The decay and dephasing rates for corresponding energy levels are $\Gamma_3 = \Gamma_4 = 2\pi \times 6\,\text{MHz}$, $\Gamma_{31} = \frac{5}{9}\Gamma_3$, $\Gamma_{32} = \frac{4}{9}\Gamma_3$, $\Gamma_{41} = \frac{4}{9}\Gamma_4$, $\Gamma_{42} = \frac{5}{9}\Gamma_4$, $\gamma_{13} = \gamma_{23} = \gamma_{14} = \gamma_{24} = 2\pi \times 3\,\text{MHz}$, and $\gamma_{12} = 2\pi \times 0.03\,\text{MHz}$. With vacuum inputs in both Stokes ($z = L$) and anti-Stokes ($z = 0$) modes, we have $\langle \hat{a}_{as}(\varpi, 0)\hat{a}_{as}^{\dagger}(\varpi', 0)\rangle = \langle \hat{a}_s(\varpi, L)\hat{a}_s^{\dagger}(\varpi', L)\rangle = \delta(\varpi - \varpi')$ and $\langle \hat{a}_{as}^{\dagger}(\varpi, 0)\hat{a}_{as}(\varpi', 0)\rangle = \langle \hat{a}_s^{\dagger}(\varpi, L)\hat{a}_s(\varpi', L)\rangle = 0$. There is also no correlation between Stokes and anti-Stokes fields at their inputs.

We numerically compute SFWM in two different regimes to confirm the consistency between the macroscopic and microscopic theories: (i) The first is the group delay regime, where the SFWM spectrum bandwidth is determined by the EIT slow-light induced phase mismatching [10]. The working parameters are $\Omega_p = 2\pi \times 1.2\,\text{MHz}$, $\Omega_c = 2\pi \times 12\,\text{MHz}$, and $\Delta_p = 2\pi \times 500\,\text{MHz}$. The cold atomic medium with length $L = 2\,\text{cm}$ has density $n = 5.1 \times 10^{16}\,\text{m}^{-3}$, corresponding to an atomic optical depth $\text{OD} = 80$ on the anti-Stokes resonance transition. (ii) The second is the Rabi oscillation regime, where biphoton correlation reveals single-atom dynamics [10]. The working parameters are $\Omega_p = 2\pi \times 1.2\,\text{MHz}$, $\Omega_c = 2\pi \times 24\,\text{MHz}$, and $\Delta_p = \omega_p - \omega_{14} = 2\pi \times 500\,\text{MHz}$. The cold atomic medium with length $L = 0.2\,\text{cm}$ has density $n = 6.4 \times 10^{14}\,\text{m}^{-3}$, corresponding to $\text{OD} = 0.1$. In both cases, we take $\Delta k = 127\,\text{rad/m}$.

The numerical results in the group delay regime are plotted in Figs. 3–5. The commutation relations $[\hat{a}_{as}(L), \hat{a}_{as}^{\dagger}(L)]$
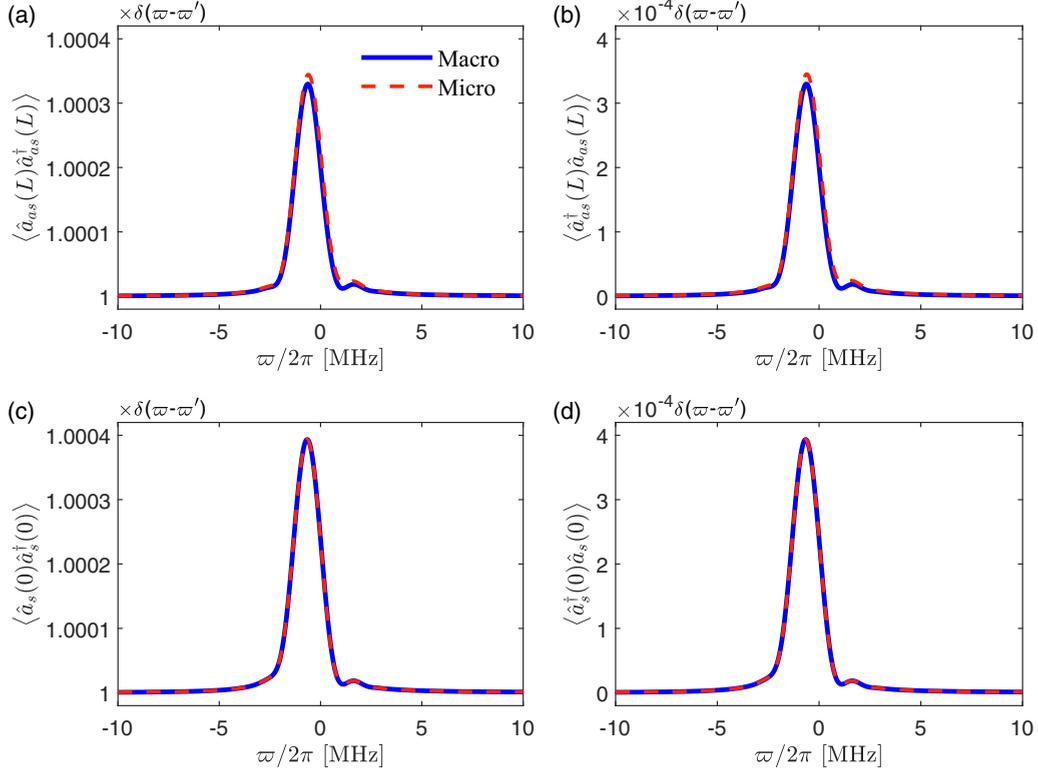
FIG. 4. Four real correlations of Stokes and anti-Stokes fields in the group delay regime: (a) $\langle \hat{a}_{as}(L)\hat{a}_{as}^\dagger(L) \rangle$, (b) $\langle \hat{a}_{as}^\dagger(L)\hat{a}_{as}(L) \rangle$, (c) $\langle \hat{a}_s(0)\hat{a}_s^\dagger(0) \rangle$, and (d) $\langle \hat{a}_s^\dagger(0)\hat{a}_s(0) \rangle$. The macroscopic (Macro) and microscopic (Micro) approaches are shown as blue solid and red dashed lines, respectively.

and $[\hat{a}_s(0), \hat{a}_s^\dagger(0)]$ are shown in Fig. 3. Macroscopic and microscopic approaches agree well with each other [Figs. 3(a) and 3(c)], with negligible relative small difference $<1.0 \times 10^{-6}$ [Figs. 3(b) and 3(d)]. As expected, the macroscopic phenomenological results give perfect flat lines at $\frac{[\hat{a}_{as}(L,\varpi),\hat{a}_{as}^\dagger(L,\varpi')]}{\delta(\varpi-\varpi')} = \frac{[\hat{a}_s(0,\varpi),\hat{a}_s^\dagger(0,\varpi')]}{\delta(\varpi-\varpi')} = 1$, which is the starting point of Sec. II. The microscopic results of field commutations are consistent with the macroscopic approach, but with $<1.0 \times 10^{-6}$ deviation at some spectra points. As we understand, these small spectra discrepancies may be caused by the ground-state and zeroth-order approximations we take for solving the microscopic Heisenberg-Langevin equations (59). If the Langevin noise operators are not taken into account, as shown in the black dotted curves in Figs. 3(a) and 3(c), the anti-Stokes commutation relation is not preserved and displays the EIT transmission spectrum, while the Stokes commutation relation still approximately holds due to the negligible gain or loss in the Stokes channel under the ground-state approximation.

Figure 4 displays four real-valued correlations of Stokes and anti-Stokes fields: (a) $\langle \hat{a}_{as}(L)\hat{a}_{as}^\dagger(L) \rangle$, (b) $\langle \hat{a}_{as}^\dagger(L)\hat{a}_{as}(L) \rangle$, (c) $\langle \hat{a}_s(0)\hat{a}_s^\dagger(0) \rangle$, and (d) $\langle \hat{a}_s^\dagger(0)\hat{a}_s(0) \rangle$. Figure 5 shows the twelve (six pairs) complex-valued correlations of Stokes and anti-Stokes fields: (a) $\langle \hat{a}_{as}(L)\hat{a}_s(0) \rangle = \langle \hat{a}_{as}^\dagger(L)\hat{a}_s^\dagger(0) \rangle^*$, (b) $\langle \hat{a}_{as}(L)\hat{a}_s(0) \rangle = \langle \hat{a}_s^\dagger(0)\hat{a}_{as}^\dagger(L) \rangle^*$, (c) $\langle \hat{a}_{as}(L)\hat{a}_s^\dagger(0) \rangle = \langle \hat{a}_s(0)\hat{a}_{as}^\dagger(L) \rangle^*$, (d) $\langle \hat{a}_s^\dagger(L)\hat{a}_s(0) \rangle = \langle \hat{a}_s^\dagger(0)\hat{a}_{as}(L) \rangle^*$, (e) $\langle \hat{a}_s(0)\hat{a}_{as}(L) \rangle = \langle \hat{a}_{as}^\dagger(L)\hat{a}_s^\dagger(0) \rangle^*$, and (f) $\langle \hat{a}_s(0)\hat{a}_s(0) \rangle = \langle \hat{a}_s^\dagger(0)\hat{a}_s^\dagger(0) \rangle^*$. The macroscopic solutions agree well with those obtained from the microscopic approach.

The numerical results in the Rabi oscillation regime are plotted in Figs. 6–8. The macroscopic phenomenological results also agree remarkably well with those from the microscopic theory.

In the microscopic Langevin-Heisenberg theory, the Stokes and anti-Stokes Langevin noise operators in Eq. (69) are expressed as a linear summation of atomic noise operators whose correlations are defined in Eq. (48). On the other side, in the macroscopic phenomenological approach [Eq. (74)], they are obtained from the noise matrix in Eq. (31) [or Eq. (15) for the forward-wave configuration] and two-mode field noise operators whose correlations follow Eq. (14). Although Eq. (69) (with atomic transition noise operators) and Eq. (74) (with two-mode optical field noise operators) appear different, their numerical results of correlations show a remarkable agreement with each other in Figs. 3–8. We attribute this to the fact that in both microscopic and macroscopic theories the two fields share the same coupling matrix, and both satisfy the bosonic commutation relations. Under these constraints, their physical observable and outputs should be uniquely determined, though the choice of noise matrix in the macroscopic phenomenological formula is not unique, for example, as elaborated on in Appendix A. It is extremely challenging to directly drive the noisematrix in Eqs. (15) and (31) from the microscopic Heisenberg-Langevin theory, because (1) the microscopic Heisenberg-Langevin theory has a huge computational complexity (see Sec. III), (2) for two systems with the same coupling matrix, their microscopic structures may be quite different, and (3) the choice of noise
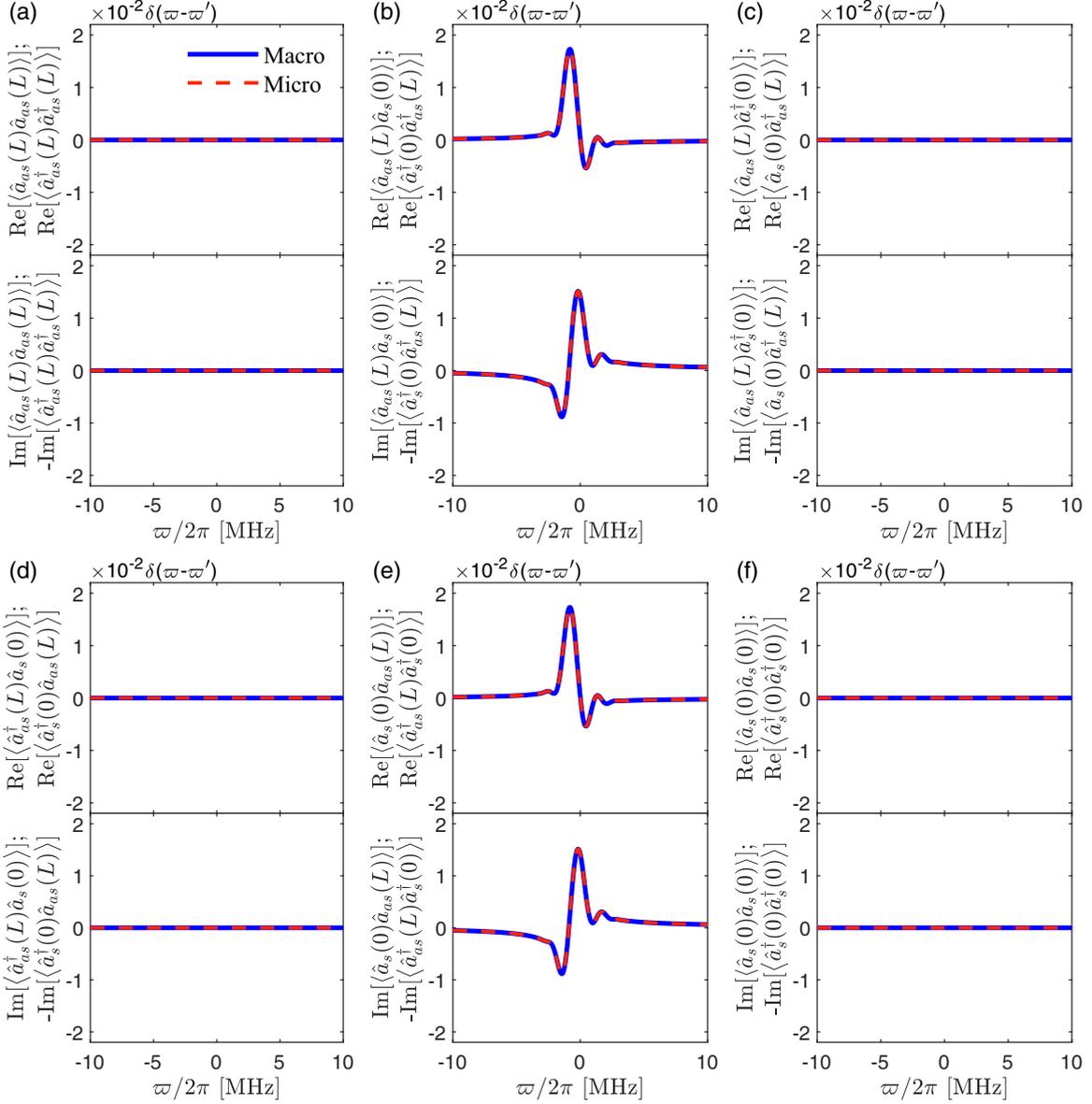
FIG. 5. Twelve complex correlations of Stokes and anti-Stokes fields in the group delay regime: (a) $\langle \hat{a}_{as}(L)\hat{a}_{as}(L)\rangle = \langle \hat{a}_{as}^\dagger(L)\hat{a}_{as}^\dagger(L)\rangle^*$, (b) $\langle \hat{a}_{as}(L)\hat{a}_s(0)\rangle = \langle \hat{a}_s^\dagger(0)\hat{a}_{as}^\dagger(L)\rangle^*$, (c) $\langle \hat{a}_{as}(L)\hat{a}_s^\dagger(0)\rangle = \langle \hat{a}_s(0)\hat{a}_{as}^\dagger(0)\rangle^*$, (d) $\langle \hat{a}_{as}^\dagger(L)\hat{a}_s(0)\rangle = \langle \hat{a}_s^\dagger(0)\hat{a}_{as}(0)\rangle^*$, (e) $\langle \hat{a}_s(0)\hat{a}_{as}(L)\rangle = \langle \hat{a}_{as}^\dagger(L)\hat{a}_s^\dagger(0)\rangle^*$, and (f) $\langle \hat{a}_s(0)\hat{a}_s(0)\rangle = \langle \hat{a}_s^\dagger(0)\hat{a}_s^\dagger(0)\rangle^*$. The macroscopic (Macro) and microscopic (Micro) approaches are shown as blue solid and red dashed lines, respectively.

matrix in the macroscopic phenomenological formula is not unique. For these reasons, we take numerical confirmation for the correlations which are relevant to the physical observables. However, we do confirm that when the nonlinear coupling coefficient is real, Eqs. (15) and (31) are indeed reduced to the known results in literature (See Cases 1 and 2 in Secs. II A and II B).

We note that although the noise field correlations from Eqs. (69) and (74) agree well with each other, there are small numerical differences at some spectral points as shown in Figs. 3–8. These neglectable discrepancies are not from fundamental physics, but rather from the approximations taken during derivation. For instance, the ground-state approximation and lowest-order perturbation are used in deriving the microscope noises and the coupling matrix. As a

result, in the microscopic Heisenberg-Langevin theory, although the underlying microscopic quantum mechanics ensures the preservation of commutation relations, the computation numerical results may be slightly away from the exact values due to these approximations. In the macroscopic phenomenological treatment, we "force" the commutation relations to hold. As a result, some adjustment is added to the Langevin noise operators to compensate the approximation-induced error in the coupling matrix. These resulted differences are small and neglectable as long as the coupling matrix describes closely its true system, as shown in Figs. 3–8.

In this work, it is assumed that the noise sources are in their ground states such that their mean occupation numbers are zero, as indicated in Eq. (14). If this condition is not met, our macroscopic phenomenological quantum Langevin
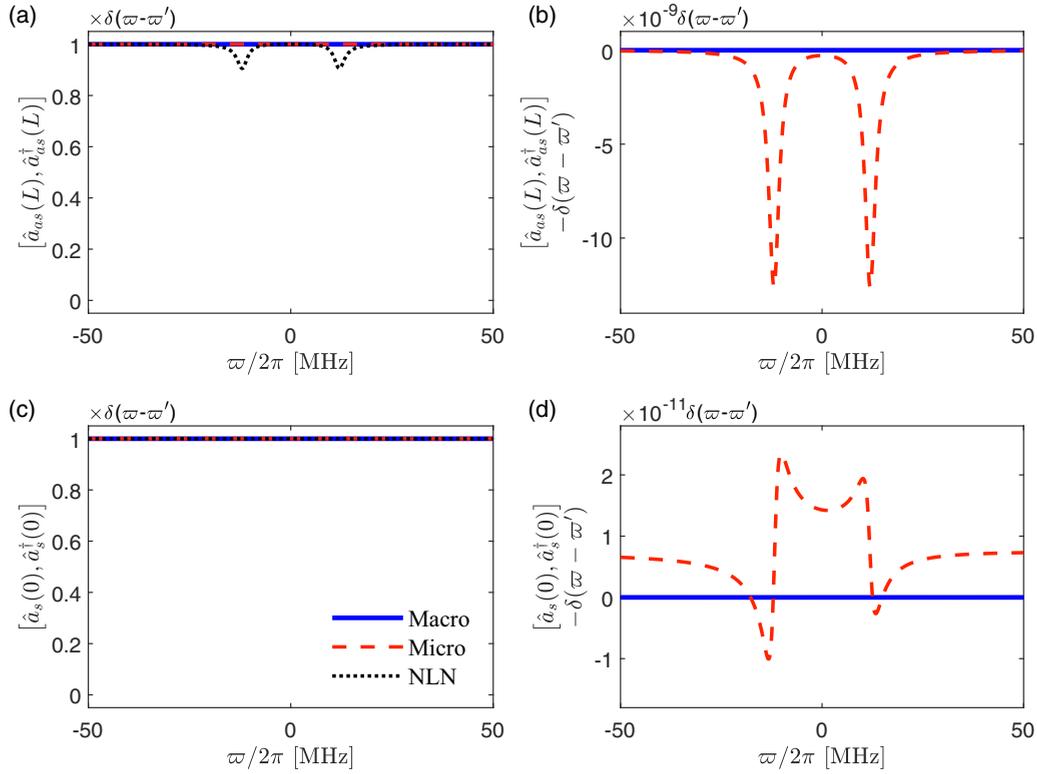
FIG. 6. Comparison of commutation relations between the macroscopic (Macro, blue solid lines) and microscopic (Micro, red dashed lines) approaches in the damped Rabi oscillation regime: (a) $[\hat{a}_{as}(L), \hat{a}_{as}^\dagger(L)]$, (b) $[\hat{a}_{as}(L), \hat{a}_{as}^\dagger(L)] - \delta(\varpi - \varpi')$, (c) $[\hat{a}_s(0), \hat{a}_s^\dagger(0)]$, and (d) $[\hat{a}_s(0), \hat{a}_s^\dagger(0)] - \delta(\varpi - \varpi')$. The results with no Langevin noise operators ("NLN") are shown as black dotted lines in (a) and (c).
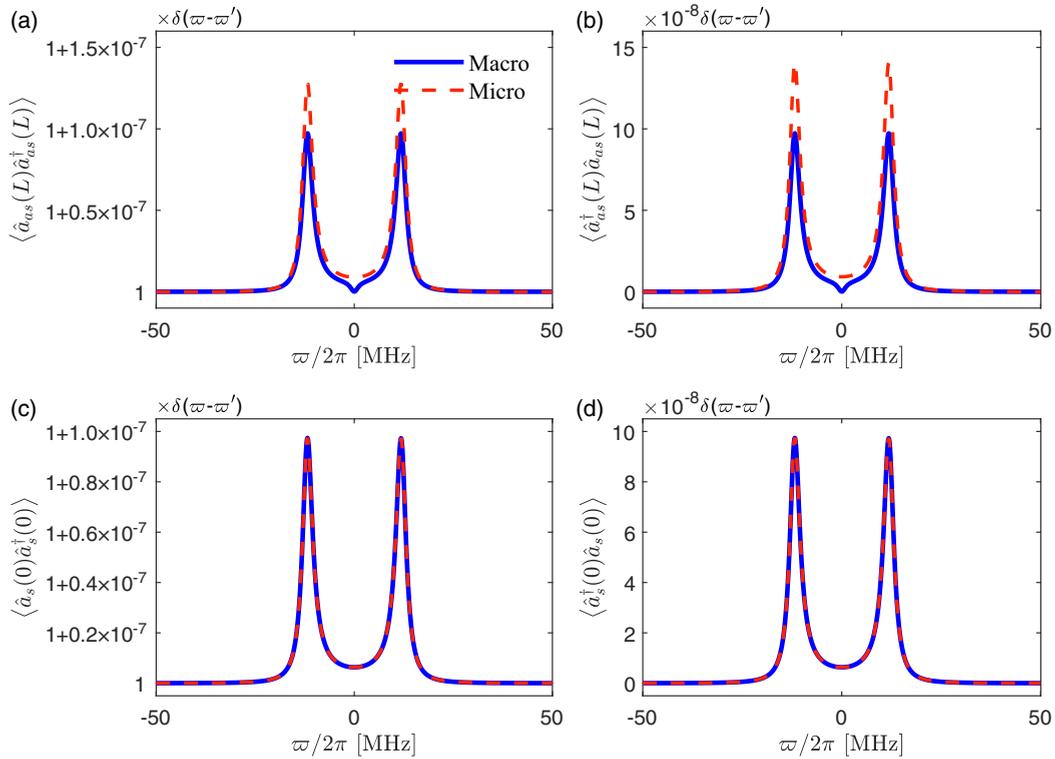

FIG. 7. Four real correlations of Stokes and anti-Stokes fields in the damped Rabi oscillation regime: (a) $\langle \hat{a}_{as}(L)\hat{a}_{as}^\dagger(L)\rangle$, (b) $\langle \hat{a}_{as}^\dagger(L)\hat{a}_{as}(L)\rangle$, (c) $\langle \hat{a}_s(0)\hat{a}_s^\dagger(0)\rangle$, and (d) $\langle \hat{a}_s^\dagger(0)\hat{a}_s(0)\rangle$. The macroscopic (Macro) and microscopic (Micro) approaches are shown as blue solid and red dashed lines, respectively.
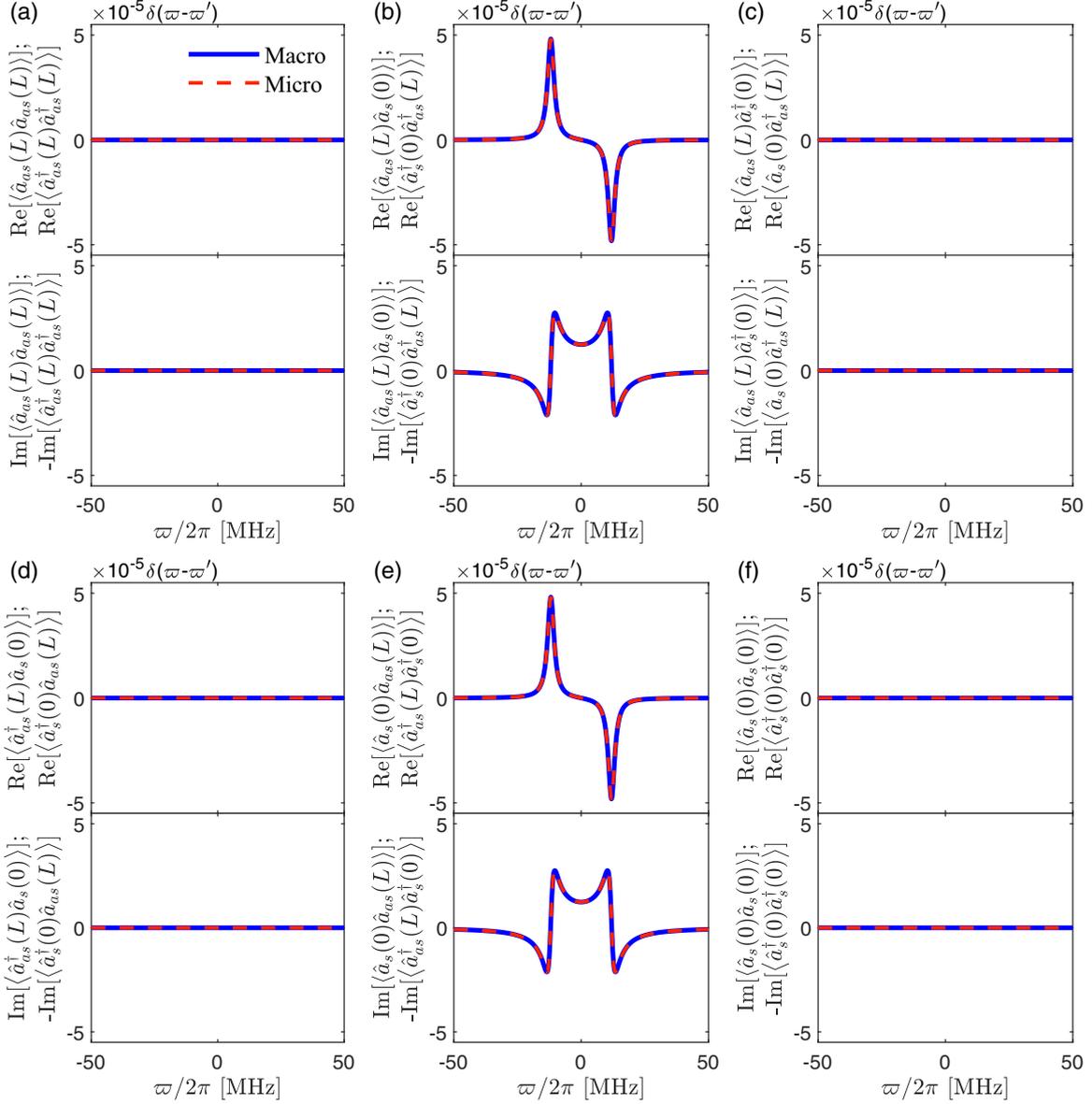
FIG. 8. Twelve complex correlations of Stokes and anti-Stokes fields in the damped Rabi oscillation regime: (a) $\langle \hat{a}_{as}(L)\hat{a}_{as}(L)\rangle = \langle \hat{a}_{as}^\dagger(L)\hat{a}_{as}^\dagger(L)\rangle^*$, (b) $\langle \hat{a}_{as}(L)\hat{a}_s(0)\rangle = \langle \hat{a}_s^\dagger(0)\hat{a}_{as}^\dagger(L)\rangle^*$, (c) $\langle \hat{a}_{as}(L)\hat{a}_s^\dagger(0)\rangle = \langle \hat{a}_s(0)\hat{a}_{as}^\dagger(L)\rangle^*$, (d) $\langle \hat{a}_{as}^\dagger(L)\hat{a}_s(0)\rangle = \langle \hat{a}_s^\dagger(0)\hat{a}_{as}(L)\rangle^*$, (e) $\langle \hat{a}_s(0)\hat{a}_{as}(L)\rangle = \langle \hat{a}_{as}^\dagger(L)\hat{a}_s^\dagger(0)\rangle^*$, and (f) $\langle \hat{a}_s(0)\hat{a}_s(0)\rangle = \langle \hat{a}_s^\dagger(0)\hat{a}_s^\dagger(0)\rangle^*$. The macroscopic (Macro) and microscopic (Micro) approaches are shown as blue solid and red dashed lines, respectively.

equations may not be applicable and require adjustment. We find that the complex nonlinear coupling coefficient arises from near-resonance interaction between light and atomic transitions. Although in this work we focus on SFWM in a double-Λ atomic system, we anticipate the same physics applies to other multiple-wave mixing processes, such as two-level [23], three-level [24–26], and diamond-shape four-level systems [27,28].

IV. BIPHOTON GENERATION

We now turn to apply the quantum Langevin theory to study time-frequency entangled photon pair (biphoton) generation through the spontaneous four-wave mixing process, especially in a variety of situations involving gain, loss, and/or complex nonlinear coupling coefficient. We consider continuous-wave pumping whose time-translation symmetry leads to frequency anticorrelation $\omega_1 + \omega_2 =$ constant between the paired photons. In the spontaneous four-wave mixing process, both input states are vacuum: $\langle \hat{a}_1^\dagger(\varpi,0)\hat{a}_1(\varpi',0)\rangle = \langle \hat{a}_2^\dagger(\varpi,0)\hat{a}_2(\varpi',0)\rangle = 0$, $\langle \hat{a}_1(\varpi',0) \hat{a}_1^\dagger(\varpi,0)\rangle = \langle \hat{a}_2(\varpi',0)\hat{a}_2^\dagger(\varpi,0)\rangle = \delta(\varpi - \varpi')$ for the forward-wave configuration, and $\langle \hat{a}_1^\dagger(\varpi,0)\hat{a}_1(\varpi',0)\rangle = \langle \hat{a}_2^\dagger(\varpi,L)\hat{a}_2(\varpi',L)\rangle = 0$, $\langle \hat{a}_1(\varpi,0)\hat{a}_1^\dagger(\varpi',0)\rangle = \langle \hat{a}_2(\varpi,L) \hat{a}_2^\dagger(\varpi',L)\rangle = \delta(\varpi - \varpi')$ for the backward-wave configuration. From Eq. (4), with $\omega_1 = \omega_{10} + \varpi$ and $\omega_2 = \omega_{20} - \varpi$,

we have

$$\hat{a}_1(t, z_1) = \frac{e^{i\omega_{10}(\frac{z_1}{c} - t)}}{\sqrt{2\pi}} \int d\varpi \, \hat{a}_1(\varpi, z_1) e^{i\varpi(\frac{z_1}{c} - t)} e^{-i\frac{\Delta k}{2} z_1},$$

$$\hat{a}_2(t, z_2) = \frac{e^{i\omega_{20}(\pm\frac{z_2}{c} - t)}}{\sqrt{2\pi}} \int d\varpi \, \hat{a}_2(\varpi, z_2) e^{-i\varpi(\pm\frac{z_2}{c} - t)} e^{-i\frac{\Delta k}{2} z_2},$$

$$(75)$$

where $\pm$ represents the forward-wave $(+)$ or backward-wave $(-)$ configuration, and $z = z_1$ and $z = z_2$ are the output positions of channels 1 and 2, respectively. For the forward-wave configuration, $z_1 = z_2 = L$. For the backward-wave configuration, $z_1 = L$ and $z_2 = 0$. The phase mismatching in vacuum $\Delta k = (\omega_{as} \pm \omega_s)/c - (\vec{k}_c + \vec{k}_p) \cdot \hat{z} \simeq (\omega_{as0} \pm \omega_{s0})/c - (\vec{k}_c + \vec{k}_p) \cdot \hat{z}$ is nearly a constant. The vacuum time delay z_i/c constants are usually very small in usual experimental conditions, so from now on we ignore these constants for simplification and rewrite the above equations to (otherwise one just needs to make a time translation $t \to t - z_i/c$)

$$\hat{a}_1(t, z_1) = \frac{e^{-i\omega_{10}t}}{\sqrt{2\pi}} \int d\varpi \, \hat{a}_1(\varpi, z_1) e^{-i\varpi t},$$

$$\hat{a}_2(t, z_2) = \frac{e^{-i\omega_{20}t}}{\sqrt{2\pi}} \int d\varpi \, \hat{a}_2(\varpi, z_2) e^{i\varpi t}.$$

$$(76)$$

The photon rate in channel m can be computed from

$$R_m \equiv \langle \hat{a}_m^\dagger(t, z_m) \hat{a}_m(t, z_m) \rangle$$

$$= \frac{1}{2\pi} \iint_{-\infty}^{\infty} d\varpi \, d\varpi' e^{-i\varpi t} e^{i\varpi' t} \langle \hat{a}_m^\dagger(\varpi', z_m) \hat{a}_m(\varpi, z_m) \rangle.$$

$$(77)$$

Here we are particularly interested in the two-photon Glauber correlation in the time domain, which can be computed from the following two different orders:

$$G_{2,1}^{(2)}(t_2, t_1) \equiv \langle \hat{a}_1^\dagger(t_1, z_1) \hat{a}_2^\dagger(t_2, z_2) \hat{a}_2(t_2, z_2) \hat{a}_1(t_1, z_1) \rangle$$

$$= |\langle \hat{a}_2(t_2, z_2) \hat{a}_1(t_1, z_1) \rangle|^2$$

$$+ |\langle \hat{a}_2^\dagger(t_2, z_2) \hat{a}_1(t_1, z_1) \rangle|^2 + R_1 R_2, \qquad (78)$$

$$G_{1,2}^{(2)}(t_1, t_2) \equiv \langle \hat{a}_2^\dagger(t_2, z_2) \hat{a}_1^\dagger(t_1, z_1) \hat{a}_1(t_1, z_1) \hat{a}_2(t_2, z_2) \rangle$$

$$= |\langle \hat{a}_1(t_1, z_1) \hat{a}_2(t_2, z_2) \rangle|^2$$

$$+ |\langle \hat{a}_2^\dagger(t_2, z_2) \hat{a}_1(t_1, z_1) \rangle|^2 + R_1 R_2, \qquad (79)$$

where we have applied the Gaussian moment theorem [29,30] to decompose the fourth-order field correlations to the sum of the products of second-order field correlations (see Supplemental Material [31] for the detailed verification). The first term in Eqs. (78) and (79) can be expressed as $|\Psi_{2,1}(t_2, t_1)|^2$ and $|\Psi_{1,2}(t_1, t_2)|^2$, where

$$\Psi_{2,1}(t_2, t_1) = \langle \hat{a}_2(t_2, z_2) \hat{a}_1(t_1, z_1) \rangle$$

$$= e^{-i\omega_{20}t_2} e^{-i\omega_{10}t_1} \psi_{2,1}(t_1 - t_2), \qquad (80)$$

$$\Psi_{1,2}(t_1, t_2) = \langle \hat{a}_1(t_1, z_1) \hat{a}_2(t_2, z_2) \rangle$$

$$= e^{-i\omega_{20}t_2} e^{-i\omega_{10}t_1} \psi_{1,2}(t_1 - t_2) \qquad (81)$$

are the two-photon wave functions with the relative parts

$$\psi_{2,1}(t_1 - t_2)$$

$$= \frac{1}{2\pi} \iint d\varpi \, d\varpi' \langle \hat{a}_2(\varpi', z_2) \hat{a}_1(\varpi, z_1) \rangle e^{-i\varpi(t_1 - t_2)},$$

$$(82)$$

$$\psi_{1,2}(t_1 - t_2)$$

$$= \frac{1}{2\pi} \iint d\varpi \, d\varpi' \langle \hat{a}_1(\varpi, z_1) \hat{a}_2(\varpi', z_2) \rangle e^{-i\varpi(t_1 - t_2)}.$$

$$(83)$$

One can show that the second term in Eqs. (78) and (79) is zero if the nonlinear coupling coefficient is real-valued, and it is usually very small as compared to other terms. The third term in Eqs. (78) and (79) is the accidental coincidence counts. The two-photon wave function and Glauber correlation satisfy the following exchange symmetry:

$$\psi_{21}(t_1 - t_2) = \psi_{2,1}(t_1 - t_2) = \psi_{1,2}(t_1 - t_2),$$

$$\Psi_{21}(t_2, t_1) = \Psi_{2,1}(t_2, t_1) = \Psi_{1,2}(t_1, t_2), \qquad (84)$$

$$G_{21}^{(2)}(t_2, t_1) = G_{2,1}^{(2)}(t_2, t_1) = G_{1,2}^{(2)}(t_1, t_2).$$

The normalized two-photon correlation is defined as

$$g_{21}^{(2)}(t_2, t_1) \equiv \frac{G_{21}^{(2)}(t_2, t_1)}{R_1 R_2}. \qquad (85)$$

As the system has time-translation symmetry with continuous-wave pumping, $G_{21}^{(2)}(t_2, t_1) = G_{21}^{(2)}(t_1 - t_2)$ depends only on the relative time $t_1 - t_2$.

A. Loss and gain

To simplify and unify the descriptions for accounting for both forward- and backward-wave cases, we define "input-output" fields: $\hat{a}_{1,\text{in}} \equiv \hat{a}_1(0)$, $\hat{a}_{2,\text{in}} \equiv \hat{a}_2(0)$, $\hat{a}_{1,\text{out}} \equiv \hat{a}_1(L)$, and $\hat{a}_{2,\text{out}} \equiv \hat{a}_2(L)$ for the forward-wave case; $\hat{a}_{1,\text{in}} \equiv \hat{a}_1(0)$, $\hat{a}_{2,\text{in}} \equiv \hat{a}_2(L)$, $\hat{a}_{1,\text{out}} \equiv \hat{a}_1(L)$, and $\hat{a}_{2,\text{out}} \equiv \hat{a}_2(0)$ for the backward-wave case. In this subsection, we aim to investigate the roles of loss and gain in biphoton generation, considering linear loss in mode 1 ($\text{Re}\{\alpha_1\} = \alpha \geqslant 0$) and linear gain ($\text{Re}\{\alpha_2\} = -g \leqslant 0$) in mode 2. We also assume κ is real, or its contribution to Langevin noises is much smaller than the linear gain and loss, i.e., $\text{Im}\{\kappa\} \ll \{\alpha, g\}$. In this case, for forward- and backward-wave configurations, the noise matrix is reduced to

$$\mathbf{N}_{\text{F,B}} = \begin{bmatrix} \sqrt{2\alpha} & 0 \\ 0 & \pm i\sqrt{2g} \end{bmatrix}. \qquad (86)$$

Hence, the output fields in Eqs. (19) and (36) can be rewritten as

$$\begin{bmatrix} \hat{a}_{1,\text{out}} \\ \hat{a}_{2,\text{out}}^\dagger \end{bmatrix} = \begin{bmatrix} A & B \\ C & D \end{bmatrix} \begin{bmatrix} \hat{a}_{1,\text{in}} \\ \hat{a}_{2,\text{in}}^\dagger \end{bmatrix} + \int_0^L \begin{bmatrix} X_{11} & X_{12} \\ X_{21} & X_{22} \end{bmatrix} \begin{bmatrix} \hat{f}_1(z) \\ \hat{f}_2(z) \end{bmatrix} dz,$$

$$(87)$$

where X_{mn} are combined coefficients. We further rewrite Eq. (87) as

$$\hat{a}_{1,\text{out}} = A\hat{a}_{1,\text{in}} + B\hat{a}_{2,\text{in}}^\dagger + \int_0^L [X_{11}\hat{f}_1(z) + X_{12}\hat{f}_2(z)],$$

$$\hat{a}_{2,\text{out}} = C^*\hat{a}_{1,\text{in}}^\dagger + D^*\hat{a}_{2,\text{in}} + \int_0^L [X_{21}^*\hat{f}_1^\dagger(z) + X_{22}^*\hat{f}_2^\dagger(z)].$$

(88)

As shown in Eq. (84), there are two different orders [$\langle: \hat{a}_2\hat{a}_1 :\rangle$ or $\langle: \hat{a}_1\hat{a}_2 :\rangle$] to compute the two-photon wave function and Glauber correlation. Although these two orders are equivalent, the numerical computation complexity may be significantly different. Computing the biphoton wave function in Eq. (83) in the order $\langle: \hat{a}_1\hat{a}_2 :\rangle$ involves nonzero noise field correlations $\langle \hat{f}_m \hat{f}_m^\dagger \rangle$, while in the order $\langle: \hat{a}_2\hat{a}_1 :\rangle$ [Eq. (82)] these noise field correlations disappear because of $\langle \hat{f}_m^\dagger \hat{f}_m \rangle = 0$. These field correlations in the frequency domain can be expressed as

$$\langle \hat{a}_{2\text{out}}(\varpi')\hat{a}_{1\text{out}}(\varpi) \rangle = \delta(\varpi - \varpi')[BD^*], \quad (89)$$

$$\langle \hat{a}_{1\text{out}}(\varpi)\hat{a}_{2\text{out}}(\varpi') \rangle$$
$$= \delta(\varpi - \varpi')\left[AC^* + \int_0^L dz(X_{11}X_{21}^* + X_{12}X_{22}^*)\right]. \quad (90)$$

Therefore, we obtain the biphoton wave function following the order $\langle: \hat{a}_2\hat{a}_1 :\rangle$

$$\psi_{21}(\tau) = \iint d\varpi\, d\varpi' \langle \hat{a}_{2,\text{out}}(\varpi')\hat{a}_{1,\text{out}}(\varpi) \rangle e^{-i\varpi\tau}$$
$$= \int d\varpi\, BD^* e^{-i\varpi\tau}, \quad (91)$$

where $\tau = t_1 - t_2$. If following the order $\langle: \hat{a}_1\hat{a}_2 :\rangle$, we have

$$\psi_{12}(\tau) = \iint d\varpi\, d\varpi' \langle \hat{a}_{1,\text{out}}(\varpi)\hat{a}_{2,\text{out}}(\varpi') \rangle e^{-i\varpi\tau}$$
$$= \int d\varpi\left[AC^* + \int_0^L dz(X_{11}X_{21}^* + X_{12}X_{22}^*)\right] e^{-i\varpi\tau}. \quad (92)$$

One can show that the second term in Eqs. (78) and (79) is zero in this loss-gain configuration. The single-channel photon rates can be obtained as

$$R_1 = \frac{1}{2\pi}\int |B|^2 d\varpi,$$
$$R_2 = \frac{1}{2\pi}\int \left[|C|^2 + \int_0^L dz(|X_{21}|^2 + |X_{22}|^2)\right] d\varpi. \quad (93)$$

It is interesting to remark that, in the loss-gain configuration, the biphoton field correlation following the order $\langle: \hat{a}_{\text{gain}}\hat{a}_{\text{loss}} :\rangle$ does not involve noise field correlations as shown in Eqs. (89) and (91), which dramatically reduces the computation complexity. On the other side, taking the order $\langle: \hat{a}_{\text{loss}}\hat{a}_{\text{gain}} :\rangle$ must include noise field correlations as shown in Eqs. (90) and (92). This may be understood in the heralded photon picture [32]: When a photon in a lossy channel is detected (annihilated) by a detector, we can always ensure there is its partner (or paired) photon in another channel; On the other side, when a photon is detected in a gain channel which produces multiple photons, we cannot always ensure
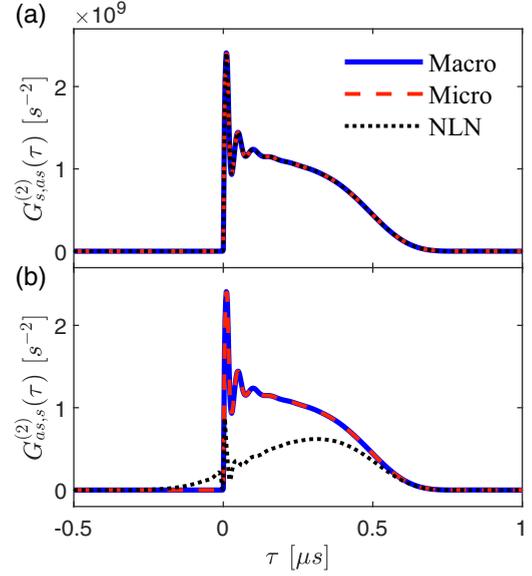

FIG. 9. Two-photon Glauber correlation in time domain in the group delay regime: (a) $G_{s,as}^{(2)}(\tau)$ and (b) $G_{as,s}^{(2)}(\tau)$. The simulation conditions are the same as those in Figs. 3–5. NLN: no Langevin noise included.

it has a partner photon in another channel. The exchange symmetry can only be preserved by taking into account the Langevin noises.

In the SFWM described in Sec. III, the anti-Stokes photons experience finite EIT loss due to the ground state dephasing ($\gamma_{12} \neq 0$), and the Stokes photons propagate with negligible but small Raman gain. Figure 9 displays the two-photon Glauber correlation in the group delay regime with the same parameters as those in Figs. 3–5. As shown in Fig. 9(a) and 9(b), both macroscopic and microscopic approaches with Langevin noises give consistent results. As expected, the computation of $G_{s,as}^{(2)}(\tau)$ (following the order $\langle: \hat{a}_s\hat{a}_{as} :\rangle$) without Langevin noise operators (black dotted line: NLN) agrees with the exact results obtained from both macroscopic (blue solid line) and microscopic (red dashed line) approaches, shown in Fig. 9(a). On the contrary, the computation of $G_{as,s}^{(2)}(\tau)$ (following the order $\langle: \hat{a}_{as}\hat{a}_s :\rangle$) without Langevin noise operators deviates significantly from the exact results, as shown in Fig. 9(b).

B. Complex phase mismatching

Different from the Heisenberg picture where the evolution of field operators is governed by their Langevin coupled equations, Ref. [10] provides a perturbation theory to describe the biphoton state in the interaction picture. The solution from the Heisenberg-Langevin theory may contain correlations of more than two photons, while the perturbation theory focuses only on the two-photon state by ignoring higher-order terms. These two treatments are expected to give the same results in the limit of small parameter gain. Although the perturbation theory in the interaction picture provides a much clear physics picture of the two-photon state, treating loss and gain requires a proper justification. In the perturbation theory, linear loss and gain are included in the complex phase mismatching

$\Delta\tilde{k}(\varpi)$ [10]. For the SFWM described in Sec. III, Ref. [10] derives the biphoton relative wave function with perturbation theory as

$$\psi(\tau) = \frac{iL}{2\pi} \int d\varpi\, \kappa(\varpi)\Phi(\varpi)e^{-i\varpi\tau}, \qquad (94)$$

where the longitudinal detuning function is

$$\Phi(\varpi) = \text{sinc}\left(\frac{\Delta\tilde{k}L}{2}\right)e^{i(k_{as}+k_s)L}. \qquad (95)$$

There is a statement in Ref. [10]: "It is found that to be consistent with the Heisenberg–Langevin theory in the low-gain limit, the argument in Φ should be replaced by $\Delta\tilde{k} = (\vec{k}_{as} + \vec{k}_s^* - \vec{k}_c - \vec{k}_p) \cdot \hat{z}$, where $\vec{k}_s^*$ is the conjugate of $\vec{k}_s$." For the SFWM in the double-Λ four-level atomic system, there is small Raman gain in the Stokes channel. What happens if there is loss in the Stokes channel? Should we take $\vec{k}_s^*$ or $\vec{k}_s$ in the complex phase mismatching $\Delta\tilde{k}(\varpi)$? Although Ref. [10] takes $\vec{k}_s^*$ for Stokes photons with gain, it is not clear whether it still holds for the case with loss. In this subsection, we not only provide a justification for the above statement in Ref. [10] from the quantum Langevin theory by taking small parametric gain approximation, but also extend the complex phase mismatching to the case with loss in the Stokes channel.

We take the same backward-wave configuration in Ref. [10]. We assume anti-Stokes photons in mode 1 are lossless with EIT and there is gain (or loss) in Stokes mode 2. The small parametric gain fulfills $|\kappa| \ll \{\alpha, g\}$.

In the backward-wave configuration, using Eqs. (7), (34), and (37), we obtain analytical expressions of A, B, C, and D as

$$A = \frac{\sqrt{q^2 - 4\kappa^2}e^{-(\alpha_1 - \alpha_2^*)L/2}}{q\sinh\left(\frac{L}{2}\sqrt{q^2 - 4\kappa^2}\right) + \sqrt{q^2 - 4\kappa^2}\cosh\left(\frac{L}{2}\sqrt{q^2 - 4\kappa^2}\right)},$$

$$B = \frac{2i\kappa}{q + \sqrt{q^2 - 4\kappa^2}\coth\left(\frac{L}{2}\sqrt{q^2 - 4\kappa^2}\right)},$$

$$C = \frac{-2i\kappa}{q + \sqrt{q^2 - 4\kappa^2}\coth\left(\frac{L}{2}\sqrt{q^2 - 4\kappa^2}\right)},$$

$$D = \frac{\sqrt{q^2 - 4\kappa^2}e^{(\alpha_1 - \alpha_2^*)L/2}}{q\sinh\left(\frac{L}{2}\sqrt{q^2 - 4\kappa^2}\right) + \sqrt{q^2 - 4\kappa^2}\cosh\left(\frac{L}{2}\sqrt{q^2 - 4\kappa^2}\right)},$$
$$(96)$$

where $q \equiv \alpha_1 + \alpha_2^* - i\Delta k$. In the small parametric gain approximation, we have

$$\sqrt{q^2 - 4\kappa^2} \approx q$$
$$= \alpha_1 + \alpha_2^* - i\Delta k = -i(\Delta k_1 - \Delta k_2^* + \Delta k) \qquad (97)$$

and

$$\alpha_1 - \alpha_2^* = -i(\Delta k_1 + \Delta k_2^*), \qquad (98)$$

where $\Delta k_m = \frac{\omega_m}{2c}\chi_m$ is the wave-number difference from that in vacuum. Hence, we simplify A, B, C, and D to

$$A = \exp[i\Delta k_1 L]\exp\left[\frac{i\Delta kL}{2}\right],$$

$$B = i\kappa L\,\text{sinc}\left[\frac{(\Delta k_1 - \Delta k_2^* + \Delta k)L}{2}\right]$$
$$\times \exp\left[\frac{i(\Delta k_1 - \Delta k_2^* + \Delta k)L}{2}\right],$$

$$C = -i\kappa L\,\text{sinc}\left[\frac{(\Delta k_1 - \Delta k_2^* + \Delta k)L}{2}\right] \qquad (99)$$
$$\times \exp\left[\frac{i(\Delta k_1 - \Delta k_2^* + \Delta k)L}{2}\right],$$

$$D = \exp[-i\Delta k_2^* L]\exp\left[\frac{i\Delta kL}{2}\right].$$

We first look at the case with gain in the Stokes (mode 2). As discussed in Sec. IV A, we take the order $\langle : \hat{a}_2\hat{a}_1 : \rangle$

$$\psi_{21}(\tau) = \iint d\varpi\, d\varpi'\langle \hat{a}_{2,\text{out}}(\varpi')\hat{a}_{1,\text{out}}(\varpi)\rangle e^{-i\varpi\tau}$$
$$= \int d\varpi\, BD^* e^{-i\varpi\tau}, \qquad (100)$$

where

$$BD^* = i\kappa L\,\text{sinc}\left[\frac{(\Delta k_1 - \Delta k_2^* + \Delta k)L}{2}\right]$$
$$\times \exp\left[\frac{i(\Delta k_1 - \Delta k_2^* + 2\Delta k_2)L}{2}\right]. \qquad (101)$$

Comparing Eqs. (100) and (101) with Eqs. (94) and (95), particularly for the argument in the sinc function, we have $\Delta\tilde{k} = \Delta k_1 - \Delta k_2^* + \Delta k = k_1 - k_2^* - k_c + k_p = k_{as} - k_s^* - k_c + k_p$, which is consistent with the statement in Ref. [10].

We now look at the case with loss in the Stokes (mode 2). We take the order $\langle : \hat{a}_1\hat{a}_2 : \rangle$ and have

$$\psi_{12}(\tau) = \iint d\varpi\, d\varpi'\langle \hat{a}_{1,\text{out}}(\varpi)\hat{a}_{2,\text{out}}(\varpi')\rangle e^{-i\varpi\tau}$$
$$= \int d\varpi\, AC^* e^{-i\varpi\tau}, \qquad (102)$$

where

$$AC^* = i\kappa^* L\,\text{sinc}\left[\frac{(\Delta k_1^* - \Delta k_2 + \Delta k)L}{2}\right]$$
$$\times \exp\left[\frac{i(2\Delta k_1 - \Delta k_1^* + \Delta k_2)L}{2}\right]. \qquad (103)$$

Comparing Eqs. (102) and (103) with Eqs. (94) and (95), we have $\Delta\tilde{k} = \Delta k_1^* - \Delta k_2 + \Delta k = k_1 - k_2 - k_c + k_p = k_{as} - k_s - k_c + k_p$, which is different from the case with gain. Here we have taken $k_1 \simeq k_1^*$ for lossless mode 1.

Although our discussion is based on the backward-wave configuration, the conclusion can be extended to the forward-wave configuration, which is derived in detail in Appendix D. Therefore, in the case with gain in the Stokes mode 2, the complex phase mismatching is $\Delta\tilde{k} = (\vec{k}_{as} + \vec{k}_s^* - \vec{k}_c - \vec{k}_p) \cdot \hat{z}$.

In the case with loss in the Stokes mode 2, the complex phase mismatching becomes $\Delta\tilde{k} = (\vec{k}_{as} + \vec{k}_s - \vec{k}_c - \vec{k}_p) \cdot \hat{z}$.

C. Complex nonlinear coupling coefficient and Rabi oscillation

As illustrated in Fig. 2, we can understand the SFWM process in the following picture. After a Stokes and anti-Stokes photon pair is born from a single atom following the atomic transitions [Fig. 2(b)], the paired photons then propagate through the medium [Fig. 2(a)]. As the photon pair can be generated at any atom inside the medium, the overall two-photon wave function (or probability amplitude) is a superposition of all possible such generation-propagation two-photon Feynman paths. Following this picture, when the propagation effect can be ignored, the biphoton state reveals the single-atom dynamics, which is connected to the nonlinear coupling coefficient. In the following, we consider SFWM in the limit of small optical depth (OD) where the linear propagation effect is small and show how the complex spectrum of nonlinear coupling coefficient reveals single-atom Rabi oscillation.

We rewrite the nonlinear coupling coefficient in Eq. (71) as

$$\kappa(\varpi) = J\left[\frac{1}{(\varpi - \Omega_e/2 + i\gamma_e)} - \frac{1}{(\varpi + \Omega_e/2 + i\gamma_e)} \right], \tag{104}$$

where

$$J = -\frac{\sqrt{\omega_{as}\omega_s}\, n\mu_{13}\mu_{24}}{8c\varepsilon_0\hbar\Omega_e} \left| \frac{\Omega_p\Omega_c}{\Delta_p + i\gamma_{14}} \right|. \tag{105}$$

Here $\Omega_e = \sqrt{|\Omega_c|^2 - (\gamma_{13} - \gamma_{12})^2}$ is the effective coupling Rabi frequency, and $\gamma_e = (\gamma_{12} + \gamma_{13})/2$ is the effective dephasing rate. Obviously, the nonlinear coupling coefficient $\kappa(\varpi)$ has a complex spectrum, with two resonances separated by the effective coupling Rabi frequency Ω_e. In the ground-state approximation with major atomic population in state $|1\rangle$, the undepleted pump laser beam is far detuned from the transition $|1\rangle \rightarrow |4\rangle$ and its excitation is weak such that we can take $\chi_s \simeq 0$. On the other side, from Eq. (70) we have the complex linear susceptibility for anti-Stokes photons

$$\chi_{as}(\varpi) = -\frac{n|\mu_{13}|^2}{\varepsilon_0\hbar} \frac{(\varpi + i\gamma_{12})}{(\varpi - \Omega_e/2 + i\gamma_e)(\varpi + \Omega_e/2 + i\gamma_e)}. \tag{106}$$

Although the anti-Stokes photon absorption at $\varpi = 0$ is suppressed by the EIT effect, there are two absorption resonances appearing at $\varpi = \pm\Omega_e/2$ which coincide with the two resonances of nonlinear coupling coefficient in Eq. (104). We take the pump laser with weak intensity ($\propto |\Omega_p|^2$) and large detuning (Δ_p) such that $\mathrm{Re}\{\alpha_{as}(\varpi = \pm\Omega_e/2)\} > \mathrm{Im}\{\kappa(\varpi = \pm\Omega_e/2)\}$, which are usually satisfied in the ground state condition. As the propagation effect is small and the phase matching is not important, the paired photons are mostly generated from the two resonances ($\varpi = \pm\Omega_e/2$) of the nonlinear coupling coefficient.

In the forward-wave configuration, with the coupling matrix

$$\mathrm{M_F} = \begin{bmatrix} -\alpha_{as} + i\frac{\Delta k}{2} & i\kappa \\ -i\kappa & -i\frac{\Delta k}{2} \end{bmatrix}, \tag{107}$$

and short medium length L satisfying $|\mathrm{M_F}L| \ll 1$, we have approximately

$$\begin{bmatrix} A & B \\ C & D \end{bmatrix} = e^{\mathrm{M_F}L} \cong \mathbb{1} + \mathrm{M_F}L$$

$$= \begin{bmatrix} 1 - \alpha_{as}L + i\frac{\Delta k}{2}L & i\kappa L \\ -i\kappa L & 1 - i\frac{\Delta k}{2}L \end{bmatrix}. \tag{108}$$

As discussed in Sec. IV A, the biphoton field correlation following the order $\langle : \hat{a}_s\hat{a}_{as} : \rangle$ does not need to count the Langevin noise operators:

$$\langle \hat{a}_s(\varpi', L)\hat{a}_{as}(\varpi, L) \rangle = BD^*\delta(\varpi - \varpi')$$

$$= i\kappa L\left(1 + i\frac{\Delta k}{2}L\right)\delta(\varpi - \varpi')$$

$$\cong i\kappa(\varpi)L\delta(\varpi - \varpi'), \tag{109}$$

where we have neglected higher-order terms $O(L^2)$. From Eq. (82), we have the relative biphoton wave function

$$\psi_{s-as}(\tau) = \frac{iL}{2\pi} \int d\varpi\, \kappa(\varpi)e^{-i\varpi\tau}, \tag{110}$$

which is the Fourier transform of the nonlinear coupling coefficient with $\tau = t_{as} - t_s$. Substituting Eq. (104) into Eq. (110), we obtain

$$\psi_{s-as}(\tau) = LJe^{-\gamma_e\tau}[e^{-i\Omega_e\tau/2} - e^{i\Omega_e\tau/2}]\Theta(\tau)$$

$$= -2iLJe^{-\gamma_e\tau}\sin\left(\frac{\Omega_e\tau}{2}\right)\Theta(\tau), \tag{111}$$

where $\Theta(\tau)$ is the Heaviside function. Equation (111) shows a damped Rabi oscillation, resulting from the beating between biphotons generated from the two resonances at $\varpi = \pm\Omega_e/2$. The Heaviside function shows that the anti-Stokes photon is always generated after its paired Stokes photon following the time order of atomic transitions $|1\rangle \rightarrow |4\rangle \rightarrow |2\rangle \rightarrow |3\rangle \rightarrow |1\rangle$ in an SFWM cycle, shown in Fig. 2(b).

In the backward-wave configuration, the coupling matrix becomes

$$\mathrm{M_B} = \begin{bmatrix} -\alpha_{as} + i\frac{\Delta k}{2} & i\kappa \\ i\kappa & -i\frac{\Delta k}{2} \end{bmatrix}. \tag{112}$$

With $|\mathrm{M_B}L| \ll 1$ we have

$$\begin{bmatrix} \bar{A} & \bar{B} \\ \bar{C} & \bar{D} \end{bmatrix} = e^{\mathrm{M_B}L} \cong \mathbb{1} + \mathrm{M_B}L$$

$$= \begin{bmatrix} 1 - \alpha_{as}L + i\frac{\Delta k}{2}L & i\kappa L \\ i\kappa L & 1 - i\frac{\Delta k}{2}L \end{bmatrix} \tag{113}$$

and

$$\begin{bmatrix} A & B \\ C & D \end{bmatrix} = \begin{bmatrix} 1 - \alpha_{as}L + i\frac{\Delta k}{2}L & i\kappa L \\ -i\kappa L & 1 + i\frac{\Delta k}{2}L \end{bmatrix}, \tag{114}$$
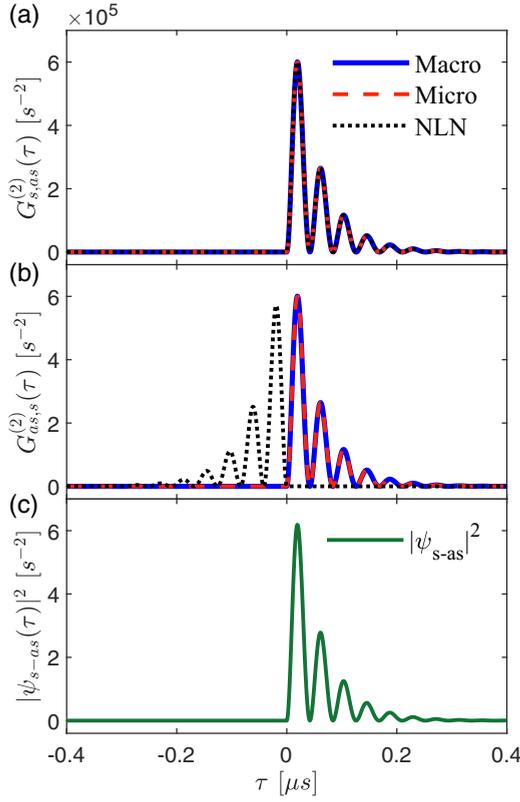
FIG. 10. Two-photon Glauber correlation in time domain in the damped Rabi oscillation regime: (a) $G_{s,as}^{(2)}(\tau)$ and (b) $G_{as,s}^{(2)}(\tau)$. The simulation conditions are the same as those in Figs. 6–8. (c) The analytic solution for the biphoton waveform $|\psi_{s-as}(\tau)|^2$. NLN: no Langevin noise included.

where we have neglect higher-order terms O(L^2). Similarly, we have

$$\langle \hat{a}_s(\varpi',0)\hat{a}_{as}(\varpi,L)\rangle \cong i\kappa(\varpi)L\delta(\varpi-\varpi'), \quad (115)$$

which is the same as Eq. (109) of the forward-wave configuration. Therefore, we obtain Rabi oscillations in both forward- and backward-wave configurations. Equation (111) is identical to the result derived from the perturbation theory in the interaction picture [10].

Figure 10 displays the two-photon Glauber correlation in the damped Rabi oscillation regime with the same parameters as those in Figs. 6–8. As illustrated in Figs. 10(a) and 10(b), both macroscopic and microscopic approaches with Langevin noises give consistent results. As expected, the computation of $G_{s,as}^{(2)}(\tau)$ (following the order $\langle : \hat{a}_s\hat{a}_{as} :\rangle$) without Langevin noise operators (dot points) agrees with the exact results obtained from both microscopic (red dashed line) and macroscopic (blue solid line) approaches, shown in Fig. 10(a). On the contrary, the computation of $G_{as,s}^{(2)}(\tau)$ (following the order $\langle : \hat{a}_{as}\hat{a}_s :\rangle$) without Langevin noise operators (dot points: NLN) deviates significantly from the exact results and violates the causality, as shown in Fig. 10(b). Figure 10(c) shows the results from the analytic solution in Eq. (111), which agree well with the exact results in Figs. 10(a) and 10(b).

It is interesting to examine a system without gain and loss whose Langevin noises are purely contributed by the complex

nonlinear coupling coefficient. In this case, the above approximation and conclusion do not hold. Let us now consider case 3 with the forward-wave configuration in Sec. II A, where $\alpha_1 = \alpha_2 = \Delta k = 0$ and $\kappa = \eta + i\zeta$. As shown in Sec. II A, the noise matrix is different as ζ is positive or negative. We first consider $\zeta > 0$, where the Langevin coupled equations (27) become

$$\frac{\partial}{\partial z}\begin{bmatrix}\hat{a}_1\\\hat{a}_2^\dagger\end{bmatrix} = \begin{bmatrix}0 & i\kappa\\-i\kappa & 0\end{bmatrix}\begin{bmatrix}\hat{a}_1\\\hat{a}_2^\dagger\end{bmatrix} + \sqrt{\zeta}\begin{bmatrix}1 & 1\\-1 & 1\end{bmatrix}\begin{bmatrix}\hat{f}_1\\\hat{f}_2^\dagger\end{bmatrix}. \quad (116)$$

Under the condition $|M_F L| \ll 1$, we solve Eq. (116) to the first order of L and have

$$\hat{a}_1(L) \cong \hat{a}_1(0) + i\kappa L\hat{a}_2^\dagger(0) + \sqrt{\zeta}\int_0^L dz(\hat{f}_1 + \hat{f}_2^\dagger),$$

$$\hat{a}_2(L) \cong \hat{a}_2(0) + i\kappa^* L\hat{a}_1^\dagger(0) + \sqrt{\zeta}\int_0^L dz(-\hat{f}_1^\dagger + \hat{f}_2). \quad (117)$$

The two-photon field correlations are

$$\langle \hat{a}_1(L)\hat{a}_2(L)\rangle = \langle \hat{a}_2(L)\hat{a}_1(L)\rangle \cong \frac{i}{2}(\kappa+\kappa^*)L\delta(\varpi-\varpi'). \quad (118)$$

As $\zeta < 0$, the Langevin coupled equations (27) become

$$\frac{\partial}{\partial z}\begin{bmatrix}\hat{a}_1\\\hat{a}_2^\dagger\end{bmatrix} = \begin{bmatrix}0 & i\kappa\\-i\kappa & 0\end{bmatrix}\begin{bmatrix}\hat{a}_1\\\hat{a}_2^\dagger\end{bmatrix} + \sqrt{-\zeta}\begin{bmatrix}1 & 1\\-1 & 1\end{bmatrix}\begin{bmatrix}\hat{f}_1^\dagger\\\hat{f}_2\end{bmatrix}. \quad (119)$$

Under the condition $|M_F L| \ll 1$, we solve Eq. (119) to the first order of L and have

$$\hat{a}_1(L) \cong \hat{a}_1(0) + i\kappa L\hat{a}_2^\dagger(0) + \sqrt{-\zeta}\int_0^L dz(\hat{f}_1^\dagger + \hat{f}_2),$$

$$\hat{a}_2(L) \cong \hat{a}_2(0) + i\kappa^* L\hat{a}_1^\dagger(0) + \sqrt{-\zeta}\int_0^L dz(-\hat{f}_1 + \hat{f}_2^\dagger). \quad (120)$$

The two-photon field correlations are

$$\langle \hat{a}_1(L)\hat{a}_2(L)\rangle = \langle \hat{a}_2(L)\hat{a}_1(L)\rangle \cong \frac{i}{2}(k+k^*)L\delta(\varpi-\varpi'), \quad (121)$$

which is the same as Eq. (118). The biphoton relative wave function is

$$\psi_{21}(\tau) = \psi_{21}^*(-\tau) = \frac{iL}{2\pi}\int d\varpi \frac{1}{2}(k+k^*)e^{-i\varpi\tau}. \quad (122)$$

One can prove that under the same limit $|M_B L| \ll 1$, the backward-wave configuration gives the same two-photon field correlation [Eqs. (118) and (121)] and temporal wave function [Eq. (122)]. Equation (122) suggests the biphoton temporal wave function has time reversal symmetry when there is no linear gain and loss.

V. CONCLUSION

In summary, we provide a macroscopic phenomenological formula of quantum Langevin equations for two coupled phase-conjugated fields with linear loss (gain) and complex nonlinear coupling coefficient, in both forward- and backward-wave configurations. The macroscopic phenomenological formula, obtained from the coupling matrix

and the requirement of preserving commutation relations of field operators during propagation, does not require knowing microscopic details of light-matter interaction and internal atomic structures. To validate this phenomenological formula, we take SFWM in a double-Λ four-level atomic system as an example to numerically confirm that our macroscopic phenomenological result is consistent with that obtained from microscopic Heisenberg-Langevin theory. As compared to the complicated microscopic theory which varies from system to system, the macroscopic coupled equations are much more friendly to experimentalists. We apply the quantum Langevin equations to study the effects of gain and/or loss as well as complex nonlinear coupling coefficient in biphoton generation, particularly to the temporal quantum correlations. We show that the computation complexity can be dramatically reduced by taking a proper order of field operators based on loss and gain. Making a comparison between the quantum

Langevin theory (in the Heisenberg picture) and the perturbation theory (in the interaction picture [10]), we extend the expression of complex phase mismatching to account for loss and gain. At last, we reveal Rabi oscillation in SFWM biphoton temporal correlation when the propagation effect is small. Although in this article we focus on biphoton generation from the spontaneous parametric process, the quantum Langevin coupled equations can also be used to study two-mode squeezing, parametric oscillation, and other quantum light state generation.

APPENDIX A: NOISE MATRIX IN BACKWARD-WAVE CONFIGURATION

In the macroscopic quantum Langevin equations, the requirement of preserving commutation relations allows multiple choices of the noise matrix. For example, $\hat{f}_1 \rightarrow -\hat{f}_1$ or/and $\hat{f}_2 \rightarrow -\hat{f}_2$ do not affect any computation results of physical observables involving pairs of Langevin noise operators. As an example, here we provide several equivalent noise matrices for backward-wave configuration:

$$
\begin{aligned}
N_{B1} &\equiv \begin{bmatrix} 1 & 0 \\ 0 & -1 \end{bmatrix} \sqrt{\begin{bmatrix} -M_{B11} & -M_{B12} \\ M_{B21} & M_{B22} \end{bmatrix} + \begin{bmatrix} -M_{B11} & -M_{B12} \\ M_{B21} & M_{B22} \end{bmatrix}^*} \\
&= \begin{bmatrix} 1 & 0 \\ 0 & -1 \end{bmatrix} N_F, \\
N_{B2} &\equiv N_{B1} \begin{bmatrix} 1 & 0 \\ 0 & -1 \end{bmatrix} \\
&= \sqrt{\begin{bmatrix} -M_{B11} & M_{B12} \\ -M_{B21} & M_{B22} \end{bmatrix} + \begin{bmatrix} -M_{B11} & M_{B12} \\ -M_{B21} & M_{B22} \end{bmatrix}^*}, \\
N_{B3} &\equiv N_{B1} \begin{bmatrix} -1 & 0 \\ 0 & 1 \end{bmatrix}, \\
N_{B4} &\equiv N_{B1} \begin{bmatrix} -1 & 0 \\ 0 & -1 \end{bmatrix} = -N_{B1}.
\end{aligned}
\tag{A1}
$$

We take the first choice N_{B1} in the main text [see Eq. (31) in Sec. II B] so that it is consistent with the microscopic treatment in Sec. III.

APPENDIX B: HEISENBERG-LANGEVIN EQUATIONS OF SFWM

The full Heisenberg equation of motion can be written as

$$
\dot{\hat{S}} = i(\hat{O}\hat{S} - \hat{S}\hat{O}) + \hat{G} + \hat{F},
\tag{B1}
$$

where

$$
\hat{S} = \begin{bmatrix}
\hat{\sigma}_{11} & \hat{\sigma}_{12} & \hat{\sigma}_{13} & \hat{\sigma}_{14} \\
\hat{\sigma}_{21} & \hat{\sigma}_{22} & \hat{\sigma}_{23} & \hat{\sigma}_{24} \\
\hat{\sigma}_{31} & \hat{\sigma}_{32} & \hat{\sigma}_{33} & \hat{\sigma}_{34} \\
\hat{\sigma}_{41} & \hat{\sigma}_{42} & \hat{\sigma}_{43} & \hat{\sigma}_{44}
\end{bmatrix},
\tag{B2}
$$

$$
\hat{O} = -\begin{bmatrix}
0 & 0 & g_{31}\hat{a}_{as} & \Omega_p/2 \\
0 & \varpi & \Omega_c/2 & g_{42}\hat{a}_s \\
g_{13}\hat{a}_{as}^* & \Omega_c^*/2 & \varpi & 0 \\
\Omega_p^*/2 & g_{24}\hat{a}_s^* & 0 & \Delta_p
\end{bmatrix},
\tag{B3}
$$

$$\hat{\mathcal{G}} = \begin{bmatrix} \Gamma_{31}\hat{\sigma}_{33} + \Gamma_{41}\hat{\sigma}_{44} & -\gamma_{12}\hat{\sigma}_{12} & -\gamma_{13}\hat{\sigma}_{13} & -\gamma_{14}\hat{\sigma}_{14} \\ -\gamma_{12}\hat{\sigma}_{21} & \Gamma_{32}\hat{\sigma}_{33} + \Gamma_{42}\hat{\sigma}_{44} & -\gamma_{23}\hat{\sigma}_{23} & -\gamma_{24}\hat{\sigma}_{24} \\ -\gamma_{13}\hat{\sigma}_{31} & -\gamma_{23}\hat{\sigma}_{32} & -\Gamma_{3}\hat{\sigma}_{33} & -\gamma_{34}\hat{\sigma}_{34} \\ -\gamma_{14}\hat{\sigma}_{41} & -\gamma_{24}\hat{\sigma}_{42} & -\gamma_{34}\hat{\sigma}_{43} & -\Gamma_{4}\hat{\sigma}_{44} \end{bmatrix}, \tag{B4}$$

$$\hat{\mathcal{F}} = \begin{bmatrix} \hat{f}_{11}^{(\sigma)} & \hat{f}_{12}^{(\sigma)} & \hat{f}_{13}^{(\sigma)} & \hat{f}_{14}^{(\sigma)} \\ \hat{f}_{21}^{(\sigma)} & \hat{f}_{22}^{(\sigma)} & \hat{f}_{23}^{(\sigma)} & \hat{f}_{24}^{(\sigma)} \\ \hat{f}_{31}^{(\sigma)} & \hat{f}_{32}^{(\sigma)} & \hat{f}_{33}^{(\sigma)} & \hat{f}_{34}^{(\sigma)} \\ \hat{f}_{41}^{(\sigma)} & \hat{f}_{42}^{(\sigma)} & \hat{f}_{43}^{(\sigma)} & \hat{f}_{44}^{(\sigma)} \end{bmatrix}. \tag{B5}$$

$\Gamma_m = \Gamma_{m1} + \Gamma_{m2}$ is the total spontaneous decay rate of excited state $|m\rangle$, where $m = 3$ or 4, and Γ_{mj} is the decay rate from state $|m\rangle$ to $|j\rangle$. For the two hyperfine ground states, there are $\Gamma_1 = \Gamma_2 = 0$. For cold atoms with only spontaneous emission decay, the dephasing rates γ_{jk} ($j \neq k$) between states $|k\rangle$ and $|j\rangle$ are $\gamma_{13} = \gamma_{23} = \Gamma_3/2$, $\gamma_{14} = \gamma_{24} = \Gamma_4/2$, $\gamma_{34} = (\Gamma_3 + \Gamma_4)/2$. γ_{12} is the dephasing rate between two hyperfine ground states $|1\rangle$ and $|2\rangle$.

APPENDIX C: MICROSCOPIC SFWM QUANTUM LANGEVIN EQUATIONS IN FORWARD-WAVE CONFIGURATION

Although Sec. III focuses on numerical confirmation of backward-wave SFWM, we remark that it may be helpful for general readers to write the SFWM quantum Langevin equations in the forward-wave configuration as well.

In the forward-wave configuration with both Stokes and anti-Stokes fields propagating along the $+z$ direction, the coupled Langevin equations become

$$\frac{\partial}{\partial z} \begin{bmatrix} \hat{a}_{as} \\ \hat{a}_s^\dagger \end{bmatrix} = M_F \begin{bmatrix} \hat{a}_{as} \\ \hat{a}_s^\dagger \end{bmatrix} + \begin{bmatrix} \hat{F}_{as} \\ \hat{F}_s^\dagger \end{bmatrix}, \tag{C1}$$

where

$$M_F = \begin{bmatrix} -\alpha_{as} + i\frac{\Delta k}{2} & i\kappa \\ -i\kappa & -\alpha_s^* - i\frac{\Delta k}{2} \end{bmatrix}, \tag{C2}$$

with $\Delta k = (\omega_{as} + \omega_s)/c - (\vec{k}_c + \vec{k}_p) \cdot \hat{z}$. The noise operators $\hat{F}_{as}$ and $\hat{F}_s^\dagger$, defined in Eq. (69), originate from microscopic atom-light interaction. To compare Eq. (C1) with Eq. (11) from the phenomenological approach in Sec. II, we take mode 1 as anti-Stokes and mode 2 as Stokes in the forward-wave configuration. From Eq. (11), we can also obtain $\hat{F}_{as}$ and $\hat{F}_s^\dagger$ from the noise matrix:

$$\begin{aligned} \hat{F}_{as} &= N_{FR11}\hat{f}_1 + N_{FI11}\hat{f}_1^\dagger + N_{FI12}\hat{f}_2 + N_{FR12}\hat{f}_2^\dagger, \\ \hat{F}_s^\dagger &= N_{FR21}\hat{f}_1 + N_{FI21}\hat{f}_1^\dagger + N_{FI22}\hat{f}_2 + N_{FR22}\hat{f}_2^\dagger. \end{aligned} \tag{C3}$$

APPENDIX D: COMPLEX PHASE MISMATCHING IN FORWARD-WAVE CONFIGURATION

In the forward-wave configuration, similar to the backward-wave configuration in Sec. IV B, we assume anti-Stokes photons in mode 1 are lossless with EIT and there is gain (or loss) in Stokes mode 2. The small parametric gain fulfills $|\kappa| \ll \{\alpha, g\}$. Using Eqs. (6) and (17), we obtain analytical expressions of A, B, C, and D as

$$A = \frac{\sqrt{q^2 + 4\kappa^2}\cosh\left(\frac{L}{2}\sqrt{q^2 + 4\kappa^2}\right) - q\sinh\left(\frac{L}{2}\sqrt{q^2 + 4\kappa^2}\right)}{\sqrt{q^2 + 4\kappa^2}e^{(\alpha_1 + \alpha_2^*)L/2}},$$

$$B = \frac{2i\kappa\sinh\left(\frac{L}{2}\sqrt{q^2 + 4\kappa^2}\right)}{\sqrt{q^2 + 4\kappa^2}e^{(\alpha_1 + \alpha_2^*)L/2}},$$

$$C = \frac{-2i\kappa\sinh\left(\frac{L}{2}\sqrt{q^2 + 4\kappa^2}\right)}{\sqrt{q^2 + 4\kappa^2}e^{(\alpha_1 + \alpha_2^*)L/2}},$$

$$D = \frac{\sqrt{q^2 + 4\kappa^2}\cosh\left(\frac{L}{2}\sqrt{q^2 + 4\kappa^2}\right) + q\sinh\left(\frac{L}{2}\sqrt{q^2 + 4\kappa^2}\right)}{\sqrt{q^2 + 4\kappa^2}e^{(\alpha_1 + \alpha_2^*)L/2}}, \tag{D1}$$

where $q \equiv \alpha_1 - \alpha_2^* - i\Delta k$. In the small parametric gain approximation, we have

$$\begin{aligned} \sqrt{q^2 - 4\kappa^2} &\approx q \\ &= \alpha_1 - \alpha_2^* - i\Delta k = -i(\Delta k_1 + \Delta k_2^* + \Delta k) \end{aligned} \tag{D2}$$

and

$$\alpha_1 + \alpha_2^* = -i(\Delta k_1 - \Delta k_2^*), \tag{D3}$$

where $\Delta k_m = \frac{\omega_m}{2c}\chi_m$ is the wave-number difference from that in vacuum. Hence, we simplify A, B, C, and D to

$$A = \exp[i\Delta k_1 L]\exp\left[\frac{i\Delta k L}{2}\right],$$

$$\begin{aligned} B = i\kappa L \,\text{sinc}&\left[\frac{(\Delta k_1 + \Delta k_2^* + \Delta k)L}{2}\right] \\ &\times \exp\left[\frac{i(\Delta k_1 - \Delta k_2^*)L}{2}\right], \end{aligned}$$

$$\begin{aligned} C = -i\kappa L \,\text{sinc}&\left[\frac{(\Delta k_1 + \Delta k_2^* + \Delta k)L}{2}\right] \\ &\times \exp\left[\frac{i(\Delta k_1 - \Delta k_2^*)L}{2}\right], \end{aligned}$$

$$D = \exp[-i\Delta k_2^* L]\exp\left[\frac{-i\Delta k L}{2}\right]. \tag{D4}$$

We first look at the case with gain in the Stokes (mode 2). As discussed in Sec. IV A, we take the order $\langle : \hat{a}_2 \hat{a}_1 : \rangle$

$$
\begin{aligned}
\psi_{21}(\tau) &= \iint d\varpi \, d\varpi' \langle \hat{a}_{2,\text{out}}(\varpi') \hat{a}_{1,\text{out}}(\varpi) \rangle e^{-i\varpi\tau} \\
&= \int d\varpi \, BD^* e^{-i\varpi\tau},
\end{aligned} \tag{D5}
$$

where

$$
\begin{aligned}
BD^* = i\kappa L \text{sinc} &\left[\frac{(\Delta k_1 + \Delta k_2^* + \Delta k)L}{2} \right] \\
&\times \exp\left[\frac{i(\Delta k_1 - \Delta k_2^* + 2\Delta k_2 + \Delta k)L}{2} \right]. \tag{D6}
\end{aligned}
$$

Comparing Eqs. (D5) and (D6) with Eqs. (94) and (95), particularly for the argument in the sinc function, we have $\Delta\tilde{k} = \Delta k_1 + \Delta k_2^* + \Delta k = k_1 + k_2^* - k_c - k_p = k_{as} + k_s^* - k_c - k_p$, which is consistent with the statement in Ref. [10].

We now look at the case with loss in the Stokes (mode 2). We take the order $\langle : \hat{a}_1 \hat{a}_2 : \rangle$ and have

$$
\begin{aligned}
\psi_{12}(\tau) &= \iint d\varpi \, d\varpi' \langle \hat{a}_{1,\text{out}}(\varpi) \hat{a}_{2,\text{out}}(\varpi') \rangle e^{-i\varpi\tau} \\
&= \int d\varpi \, AC^* e^{-i\varpi\tau},
\end{aligned} \tag{D7}
$$

where

$$
\begin{aligned}
AC^* = i\kappa^* L \text{sinc} &\left[\frac{(\Delta k_1^* + \Delta k_2 + \Delta k)L}{2} \right] \\
&\times \exp\left[\frac{i(2\Delta k_1 - \Delta k_1^* + \Delta k_2 + \Delta k)L}{2} \right]. \tag{D8}
\end{aligned}
$$

Comparing Eqs. (D7) and (D8) with Eqs. (94) and (95), we have $\Delta\tilde{k} = \Delta k_1^* + \Delta k_2 + \Delta k = k_1 + k_2 - k_c + k_p = k_{as} + k_s - k_c - k_p$, which is different from the case with gain. Here we have taken $k_1 \simeq k_1^*$ for lossless mode 1. Therefore, in the case with loss in the Stokes mode 2, the complex phase mismatching becomes $\Delta\tilde{k} = (\vec{k}_{as} + \vec{k}_s - \vec{k}_c - \vec{k}_p) \cdot \hat{z}$.

[1] C. W. Gardiner and M. J. Collett, Input and output in damped quantum systems: Quantum stochastic differential equations and the master equation, Phys. Rev. A **31**, 3761 (1985).

[2] M. O. Scully and M. S. Zubairy, *Quantum Optics* (Cambridge University Press, Cambridge, 1997).

[3] Y. Yamamoto and A. Imamoglu, Mesoscopic Quantum Optics (Wiley, New York, 1999).

[4] C. Gardiner and P. Zoller, *Quantum Noise: A Handbook of Markovian and Non-Markovian Quantum Stochastic Methods with Applications to Quantum Optics* (Springer Science & Business Media, Berlin, 2004).

[5] R. Benguria and M. Kac, Quantum Langevin Equation, Phys. Rev. Lett. **46**, 1 (1981).

[6] R. W. Boyd, *Nonlinear Optics* (Academic, New York, 2020).

[7] S. Shwartz, R. N. Coffee, J. M. Feldkamp, Y. Feng, J. B. Hastings, G. Y. Yin, and S. E. Harris, X-Ray Parametric Down-Conversion in the Langevin Regime, Phys. Rev. Lett. **109**, 013602 (2012).

[8] U. A. Javid and Q. Lin, Quantum correlations from dynamically modulated optical nonlinear interactions, Phys. Rev. A **100**, 043811 (2019).

[9] G. Shafiee, D. V. Strekalov, A. Otterpohl, F. Sedlmeir, G. Schunk, U. Vogl, H. G. L. Schwefel, G. Leuchs, and C. Marquardt, Nonlinear power dependence of the spectral properties of an optical parametric oscillator below threshold in the quantum regime, New J. Phys. **22**, 073045 (2020).

[10] S. Du, J. Wen, and M. H. Rubin, Narrowband biphoton generation near atomic resonance, J. Opt. Soc. Am. B **25**, C98 (2008).

[11] P. Kolchin, Electromagnetically-induced-transparency-based paired photon generation, Phys. Rev. A **75**, 033814 (2007).

[12] L. Zhao, Y. Su, and S. Du, Narrowband biphoton generation in the group delay regime, Phys. Rev. A **93**, 033815 (2016).

[13] C. H. Raymond Ooi, Q. Sun, M. S. Zubairy, and M. O. Scully, Correlation of photon pairs from the double Raman amplifier: Generalized analytical quantum Langevin theory, Phys. Rev. A **75**, 013820 (2007).

[14] Y. Jiang, Y. Mei, Y. Zuo, Y. Zhai, J. Li, J. Wen, and S. Du, Anti-Parity-Time Symmetric Optical Four-Wave Mixing in Cold Atoms, Phys. Rev. Lett. **123**, 193604 (2019).

[15] Y. Mei, X. Guo, L. Zhao, and S. Du, Mirrorless Optical Parametric Oscillation with Tunable Threshold in Cold Atoms, Phys. Rev. Lett. **119**, 150406 (2017).

[16] X.-W. Luo, C. Zhang, and S. Du, Quantum Squeezing and Sensing with Pseudo-Anti-Parity-Time Symmetry, Phys. Rev. Lett. **128**, 173602 (2022).

[17] C. M. Bender and S. Boettcher, Real Spectra in Non-Hermitian Hamiltonians Having PT Symmetry, Phys. Rev. Lett. **80**, 5243 (1998).

[18] M.-A. Miri and A. Alù, Exceptional points in optics and photonics, Science **363**, eaar7709 (2019).

[19] D. A. Braje, V. Balić, S. Goda, G. Y. Yin, and S. E. Harris, Frequency Mixing Using Electromagnetically Induced Transparency in Cold Atoms, Phys. Rev. Lett. **93**, 183601 (2004).

[20] V. Balić, D. A. Braje, P. Kolchin, G. Y. Yin, and S. E. Harris, Generation of Paired Photons with Controllable Waveforms, Phys. Rev. Lett. **94**, 183601 (2005).

[21] S. E. Harris, Electromagnetically induced transparency, Phys. Today **50**, 36 (1997).

[22] M. Fleischhauer, A. Imamoglu, and J. P. Marangos, Electromagnetically induced transparency: Optics in coherent media, Rev. Mod. Phys. **77**, 633 (2005).

[23] S. Du, J. Wen, M. H. Rubin, and G. Y. Yin, Four-Wave Mixing and Biphoton Generation in a Two-Level System, Phys. Rev. Lett. **98**, 053601 (2007).

[24] P. Kolchin, S. Du, C. Belthangady, G. Y. Yin, and S. E. Harris, Generation of Narrow-Bandwidth Paired Photons: Use of a Single Driving Laser, Phys. Rev. Lett. **97**, 113602 (2006).

[25] S. Du, E. Oh, J. Wen, and M. H. Rubin, Four-wave mixing in three-level systems: Interference and entanglement, Phys. Rev. A **76**, 013803 (2007).

[26] H. Yan, S. Zhang, J. F. Chen, M. M. T. Loy, G. K. L. Wong, and S. Du, Generation of Narrow-Band Hyperentangled

Nondegenerate Paired Photons, Phys. Rev. Lett. **106**, 033601 (2011).

[27] R. T. Willis, F. E. Becerra, L. A. Orozco, and S. L. Rolston, Four-wave mixing in the diamond configuration in an atomic vapor, Phys. Rev. A **79**, 033814 (2009).

[28] D. J. Whiting, R. S. Mathew, J. Keaveney, C. S. Adams, and I. G. Hughes, Four-wave mixing in a non-degenerate four-level diamond configuration in the hyperfine Paschen-Back regime, J. Mod. Opt. **65**, 713 (2018).

[29] L. Mandel and E. Wolf, *Optical Coherence and Quantum Optics* (Cambridge University Press, Cambridge, 1995).

[30] W. H. Louisell, *Quantum Statistical Properties of Radiation* (Wiley, New York, 1973).

[31] See Supplemental Material at http://link.aps.org/supplemental/10.1103/PhysRevA.107.053703 for the detailed verification of Eqs. (78) and (79).

[32] S. Du, Quantum-state purity of heralded single photons produced from frequency-anticorrelated biphotons, Phys. Rev. A **92**, 043836 (2015).